



INTERNATIONAL ATOMIC ENERGY AGENCY  
UNITED NATIONS EDUCATIONAL, SCIENTIFIC AND CULTURAL ORGANIZATION  
**INTERNATIONAL CENTRE FOR THEORETICAL PHYSICS**  
I.C.T.P., P.O. BOX 586, 34100 TRIESTE, ITALY, CABLE: CENTRATOM TRIESTE



UNITED NATIONS INDUSTRIAL DEVELOPMENT ORGANIZATION



**INTERNATIONAL CENTRE FOR SCIENCE AND HIGH TECHNOLOGY**

c/o INTERNATIONAL CENTRE FOR THEORETICAL PHYSICS 34100 TRIESTE (ITALY) VIA GRIGNANO, 9 (ADRIATICO PALACE) P.O. BOX 586 TELEPHONE 040-224572 TELEFAX 040-224575 TELEX 460449 APH I

H4.SMR/676-13

**SECOND SCHOOL ON THE USE OF SYNCHROTRON  
RADIATION IN SCIENCE AND TECHNOLOGY:  
"JOHN FUGGLE MEMORIAL"**

**25 October - 19 November 1993**

*Miramare - Trieste, Italy*

***Reality: Tangent errors and Thermal Loads***

**C. Lenardi**  
**Consorzio IMFM, Unità Politecnico di Milano**  
**Italy**

# **Reality:**

## **Tangent errors and Thermal Loads**

**C. Lenardi**

*Consorzio INFM, Unità Politecnico di Milano, p.zza Leonardo da Vinci 32,  
I-20133 Milano, Italy.*

Second School on the Use of Synchrotron Radiation  
in Science and Technology: "John Fuggle Memorial"

Trieste (IT), 25 October -19 November 1993.

# Introduction

Third generation synchrotron radiation sources deliver VUV/X-ray beams of unprecedented quality and power. Can the beam features be conserved downstream to the experiments?

## Conservation of emittance

The tolerable increase of emittance by the optics should be comparable to the stability specifications of the source parameters expected from the machine (e.g.  $\pm 10\%$  source size and beam divergence).

a) *fundamental limits*

- optical aberrations

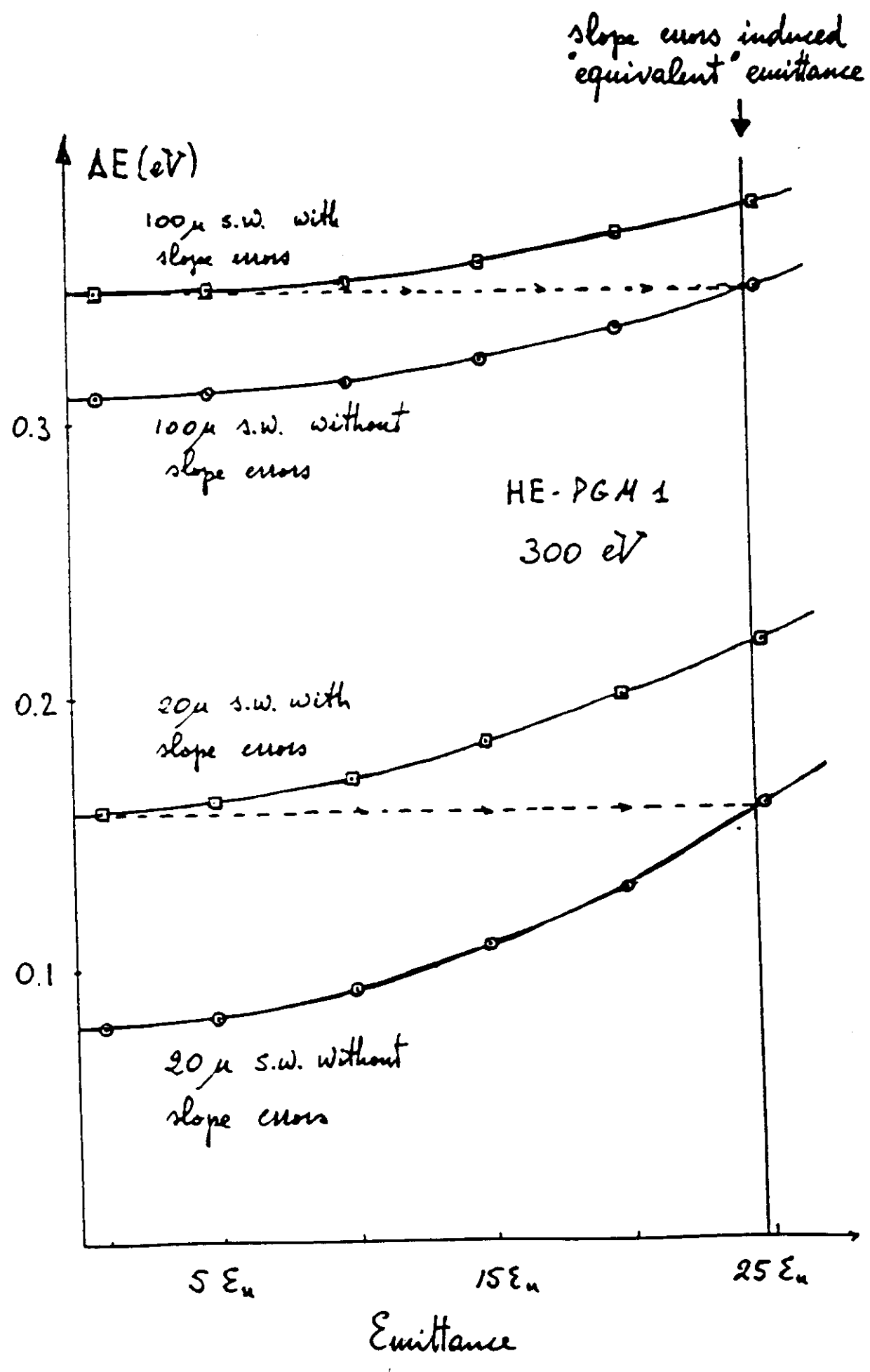
b) *technological limits*

- surface quality of mirrors/gratings
- quality of single crystals
- strain-free mechanical mounting
- stability of the optical element

# Surface quality

- Roughness  
Few Å rms (state-of-the-art: feasible!)
- Slope errors  
1÷2  $\mu$ rad

Type of mirror	Standard	Special	Prospective
flat	0.5"	0.2"	0.02"
spheric	1÷2"	0.5"	
aspheric	4÷5"	1÷2	0.5"



## Conservation of brilliance

Thermally-induced slope errors and defective manufacturing of the optical elements yield a loss of brilliance, by far the acceptable tolerances. Thus a reduction of thermal distortions and figure errors are of fundamental relevance for preserving beam brilliance.

- The vertical source size is smaller than horizontal source size, thus for having high energy resolution the dispersive plane should be vertical, and thus the **vertical brilliance should be conserved**.
- In grazing incidence the influence of **sagittal and tangential errors** at the image plane are different.

# Slope errors

- Reflection law:

$$\hat{r} = \hat{i} - 2(\hat{i} \cdot \hat{n})\hat{n}$$

$\hat{i}$  verson of the incident beam

$\hat{r}$  verson of the reflected beam

$\hat{n}$  verson of the normal to the surface

- Local variation of the normal  $\delta\vec{n}$  implies a variation of the reflected beam:

$$\delta\vec{r} = -2[(\hat{i} \cdot \delta\vec{n})\hat{n} + (\hat{i} \cdot \hat{n})\delta\vec{n}]$$

- The deviation  $|\delta\vec{r}_t|$  in the tangential plane due to a variation  $|\delta\vec{n}| = \delta\varphi$  is given by:

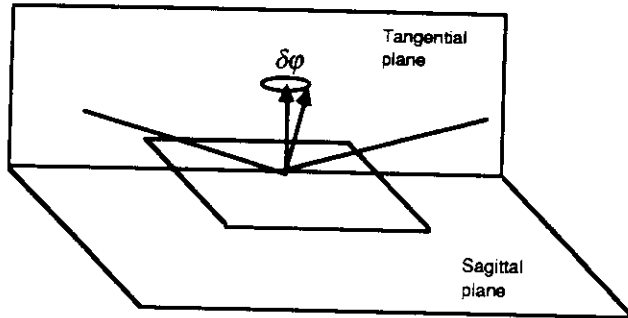
$$|\delta\vec{r}_t| = 2\sqrt{(\hat{i} \cdot \delta\vec{n})^2 + (\hat{i} \cdot \hat{n})^2 |\delta\vec{n}|^2} = 2\sqrt{\sin^2 \alpha (\delta\varphi)^2 + \cos^2 \alpha (\delta\varphi)^2} = 2\delta\varphi$$

- The deviation  $|\delta\vec{r}_s|$  in the sagittal plane due to a variation  $|\delta\vec{n}| = \delta\varphi$  ( $\hat{i} \cdot \delta\vec{n} = 0$ ) is given by:

$$|\delta\vec{r}_s| = 2\sqrt{(\hat{i} \cdot \hat{n})^2 |\delta\vec{n}|^2} = 2\cos \alpha (\delta\varphi)$$

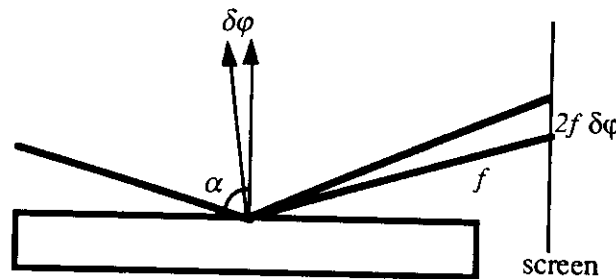
$|\delta\vec{r}_s|$  depends on the incident angle

- We suppose the distribution of slope errors to be gaussian:  $\sigma = \delta\gamma$  (rms value). If the angular variation of the normal in tangential and sagittal planes are equal, it follows that  $\delta\gamma = \sqrt{2} \delta\varphi$ .



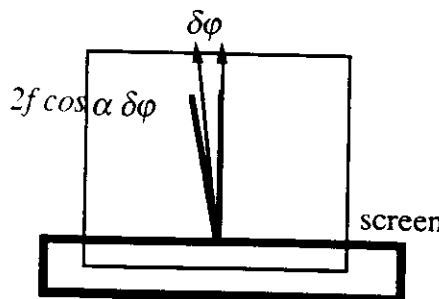
- aberration in the tangential plane:

$$\Delta z = 2f \delta\varphi$$



- aberration in the sagittal plane:

$$\Delta y = 2f \cos \alpha \delta\varphi$$



*Example:*

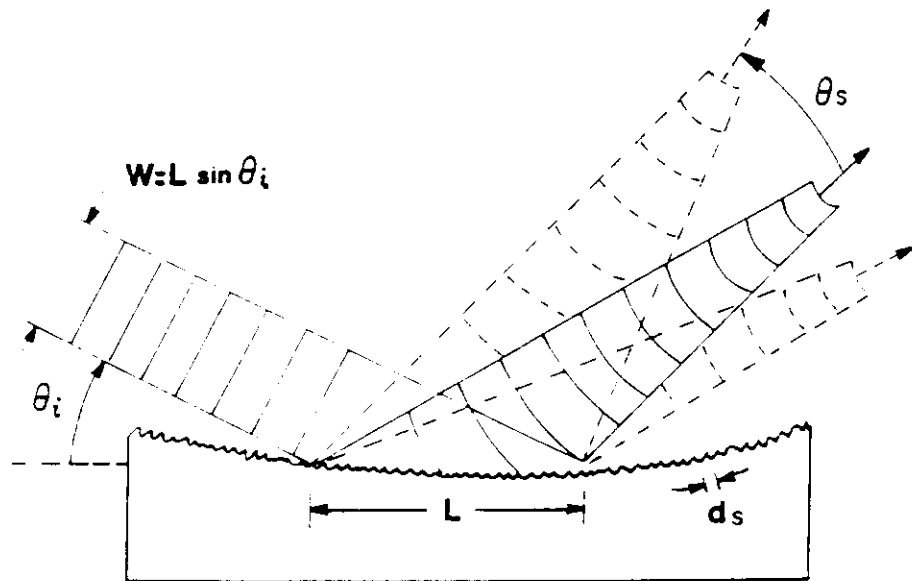
incident angle  $\alpha = 87$  deg

rms value of surface slope errors  $\delta\gamma = 1$  arcsec ( $\sim 5$   $\mu$ rad)

focal distance  $f = 3$  m

$$\Delta z = 21.2 \text{ } \mu\text{m rms}$$

$$\Delta y = 1.11 \text{ } \mu\text{m rms}$$



$$\theta_s = \frac{\lambda}{d_s \theta_i}$$

An X-ray beam impinging upon a mirror surface at an incidence angle  $\theta_i$  may be specularly reflected or scattered away from the specular beam by an amount  $\theta_s$ . In this one-dimensional illustration, the angular deviation is related to the surface spatial period,  $d_s$ , through the grating equation (Takacs 1986).

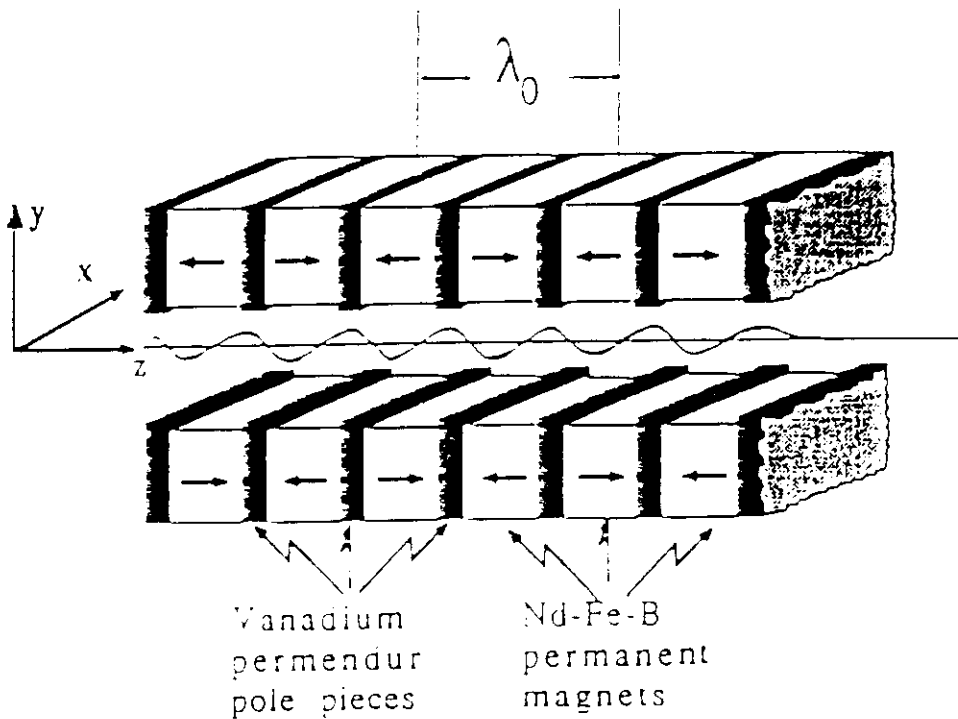
# Heat loading

- Third generation synchrotron radiation sources will deliver radiation beams with *unprecedented power densities*. In particular multipolar magnetic devices, such as undulators and wigglers, will increase the brilliance of 4÷5 order of magnitude.
- Beamlime performance depends critically on *thermally-induced deformations* (besides manufacturing slope errors).

# Heat loading effects

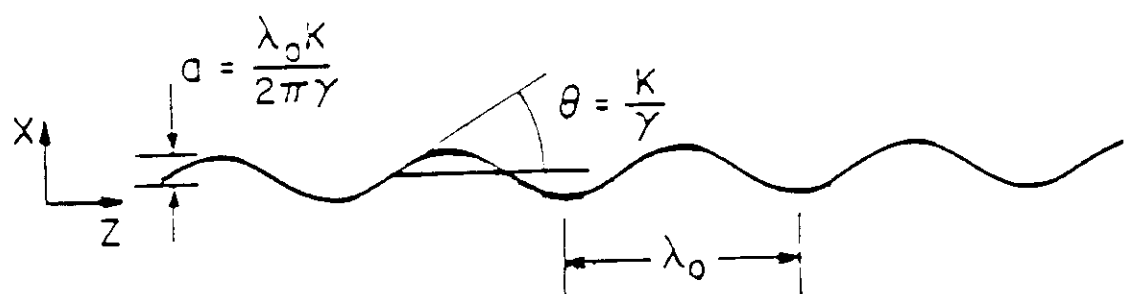
- Degradation of the optical properties of beamline reflecting/diffracting components:
  - thermally induced deformations on optical surfaces produce focal image broadening and/or shift;
  - large amount of absorbed power upsets the designed optical figure.
- Radiation damage.
- Breaking of the optical element.
- Total detrimental effects:
  - **loss in photon flux**
  - **loss in energy resolution**

## INSERTION DEVICES TYPICAL STRUCTURE



$$B = B_0 \cos(2\pi z/\lambda_0)$$

$B_0$  (T) Peak Field at Poles



DEFLECTION PARAMETER    $K = 0.934 \lambda_0 B_0$   
 PARTICLE TRAJECTORY DETERMINES DEVICE  
 CHARACTERISTICS

# Total power for an ID source

$$P_{tot} [\text{W}] = 1.263 E_b^2 \langle B^2 \rangle I L$$

$$\langle B^2 \rangle \approx \frac{B_0^2}{2}$$

$E_b$  storage ring energy [GeV]

$B$  magnetic field [T]

$I$  stored current [mA]

$L$  ID length [m]

# Angular distribution of power

(zero emittance)

$$\frac{d^2P}{d\theta d\psi} [\text{W} \cdot \text{rad}^2] = P_{tot} \frac{21\gamma^2}{16\pi K} G(K) f_K(\gamma\theta, \gamma\psi)$$

$$\frac{d^2P}{d\theta d\psi} [\text{W} \cdot \text{mrad}^2] = 10.84 B_0 E_b^4 N G(K) f_K(\gamma\theta, \gamma\psi)$$

$\theta$  horizontal observation angle

$\psi$  vertical observation angle

$N$  number of magnet periods

$I$  stored current [A]

$\gamma$  electron energy/m<sub>e</sub>c<sup>2</sup>

$\gamma = 1957 E_b$  [GeV]

$K$  deflection parameter

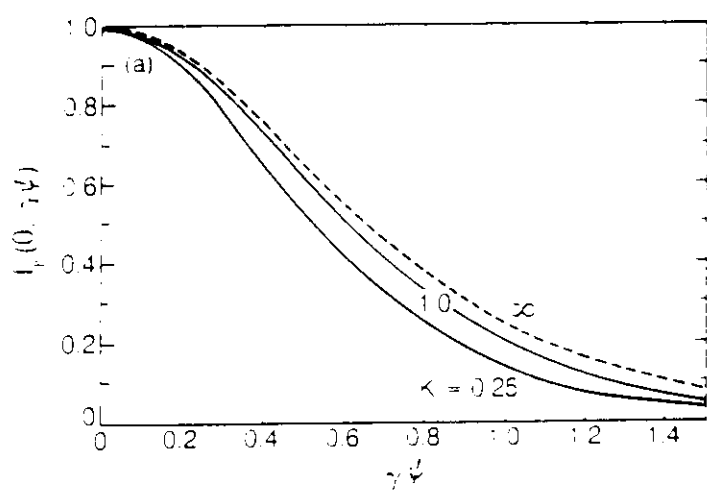
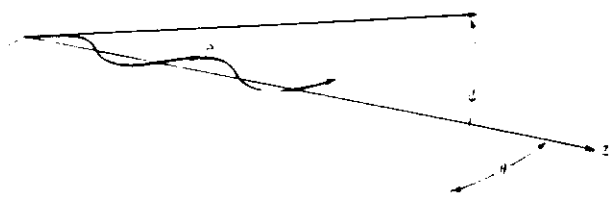
$K = 0.934 \lambda_0 [\text{cm}] B_0$

$G(K)$  angle independent factor

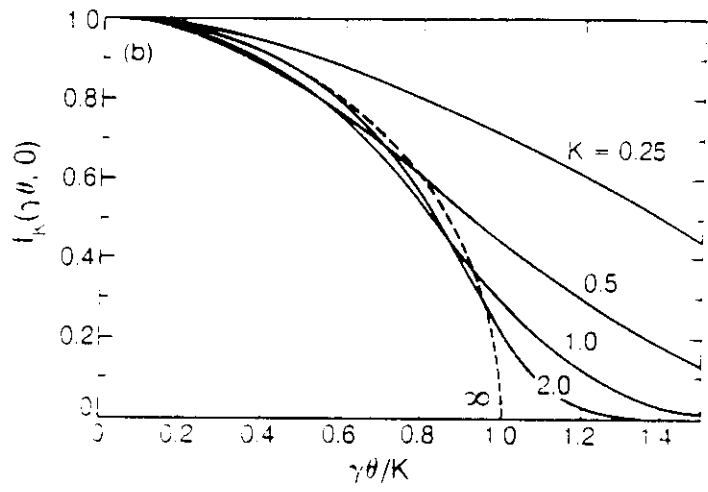
$G(K) \rightarrow 1$  as  $K$  increases from 0

$f_K(\gamma\theta, \gamma\psi)$  normalized angular distribution function

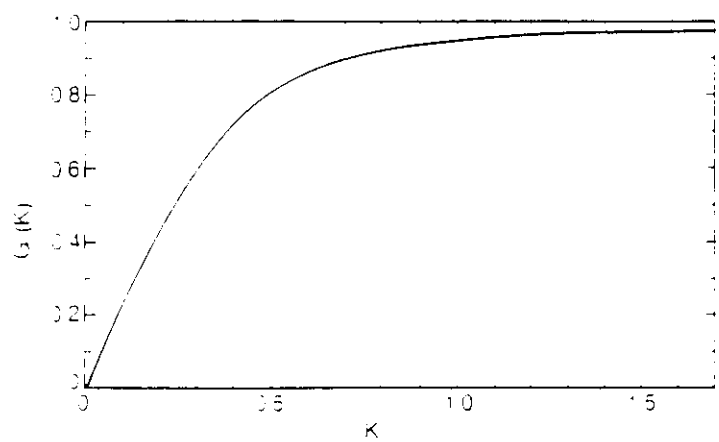
$f_K(0,0) = 1$  (on-axis, peak power density)



The behavior of the function  $f_K(0, \gamma\psi)$ .



The behavior of the function  $f_K(\gamma\theta, 0)$ .



The behavior of the function  $G(K)$ .

# Angular distribution function

The power envelope depends on the deflection parameter  $K$ .

Horizontal  $\theta$  direction

$$\pm K / \gamma$$

Vertical  $\psi$  direction

$$\pm 1 / \gamma$$

If the ID works in the range of undulator mode ( $K \leq 1$ ) the angular distribution of the  $n$ th harmonic is concentrated in a narrow cone whose half-width is given by:

$$\sigma_{\theta, \psi} \approx \sqrt{\frac{\lambda_n}{L}} = \frac{1}{\gamma} \sqrt{\frac{1+K^2/2}{2nN}}$$

$n$  harmonic number

$\lambda_n$  wavelength of  $n$ th harmonic

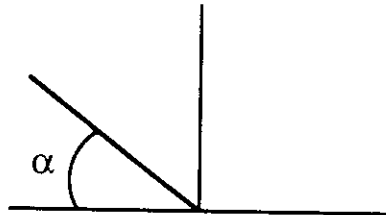
# Power density per unit area

## Normal incidence

$$\frac{d^2P}{dA} [\text{W} \cdot \text{mm}^2] = \frac{d^2P}{d\theta d\psi} [\text{W} \cdot \text{rad}^2] \frac{1}{R^2}$$

$R$  [m] distance from ID source

## For a given impinging angle $\alpha$



- Reduction of the power density by  $\sin(\alpha)$

## Footprint

- For normal incidence: half-widths of the spot

$$\sigma_x = \sigma_\theta R$$

$$\sigma_y = \sigma_\psi R$$

- For  $\alpha$  impinging angle: an increment by  $1/\sin(\alpha)$

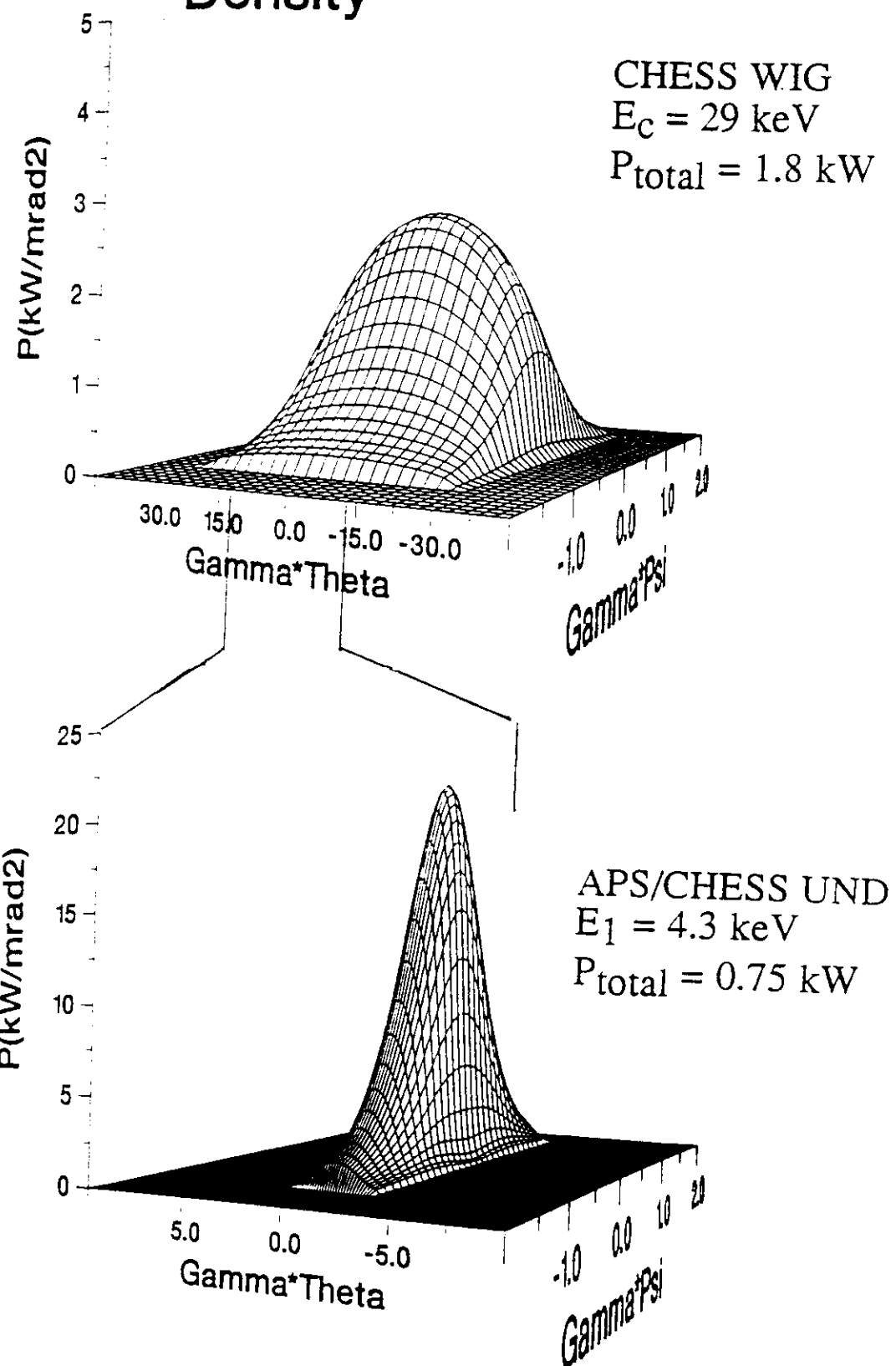
# RELEVANT!

$$P_{tot} \sim E_b^2$$
$$\frac{d^2 P}{d\theta d\psi} \sim E_b^4$$

## TYPICAL ID PEAK POWER DENSITIES

	NSLS	SSRL	PEP	CHESS	APS	ALS					
SUW	US	VI	X	UND	WIG	UND	UND $\wedge$	WIGA	U5	W13.6	
x-ray	vuv										
$B_0(T)$	6	0.45	1.3	1.3	0.2	1.0	0.45	0.8	1.0	0.95	1.0
Poles	6	63	54	31	52	6	123	300	20	200	32
Length(m)	0.53	2.4	1.96	2.0	2.0	1.05	2.0	5.0	1.5	5.0	2.2
K	99	3	8	15	3	30	1.4	2.5	15	4	13
P <sub>total</sub> (kW)	38	0.1	1.5	1.6	0.3	1.8	0.75	9.8	4.6	2.5	1.5
P(kW/mrad <sup>2</sup> )	3.8	0.03	2.7	1.5	10	2.7	25	300	24	2.3	0.36
P(W/mm <sup>2</sup> ) @ 10 m	38	0.3	27	15	100	27	244	3000	240	23	3.6
$\sigma'(v)$ mrad	0.12	0.4	0.1	0.1	0.04	0.06	0.06	0.044	0.044	0.2	0.2
$\sigma'(h)$ mrad	20	2.	1.36	2.5	0.2	3	0.14	0.18	1.1	1.36	5.0

# Angular Power Density



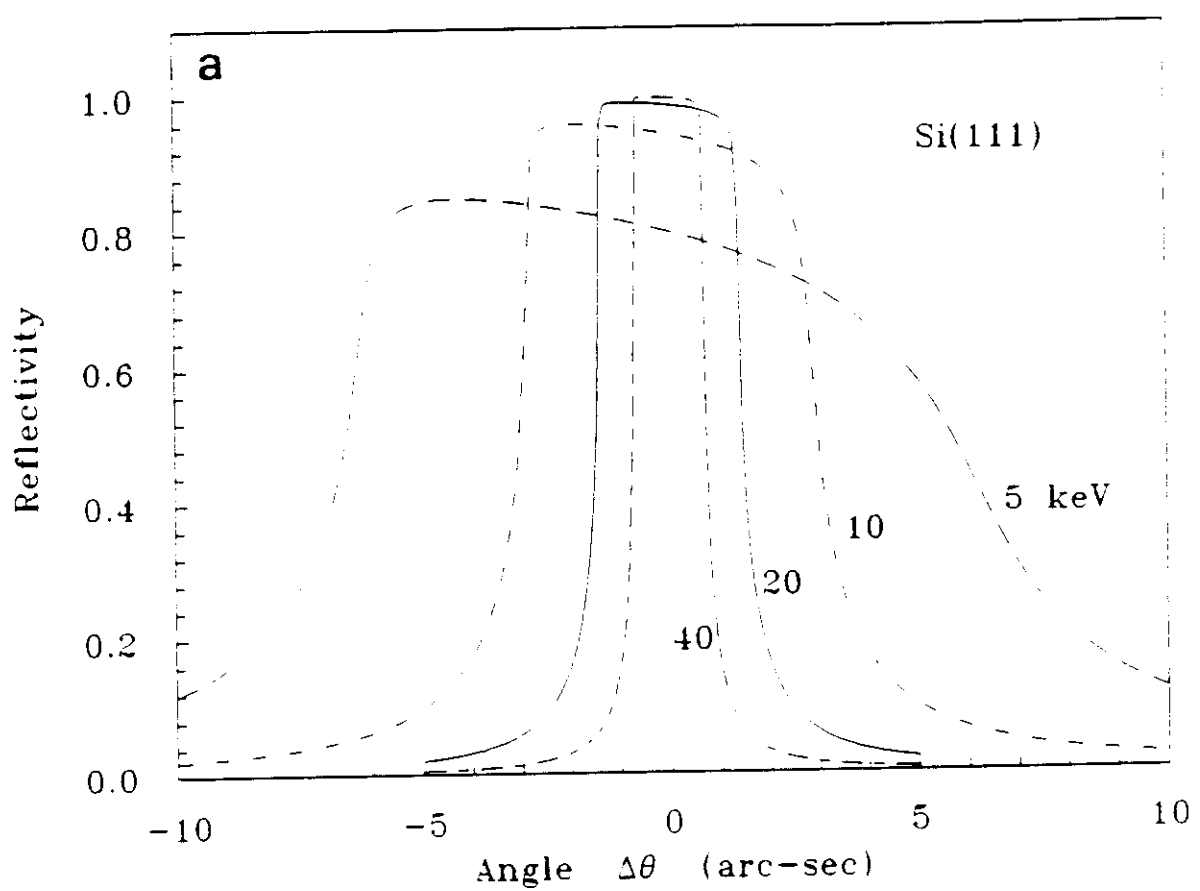
# First optical element

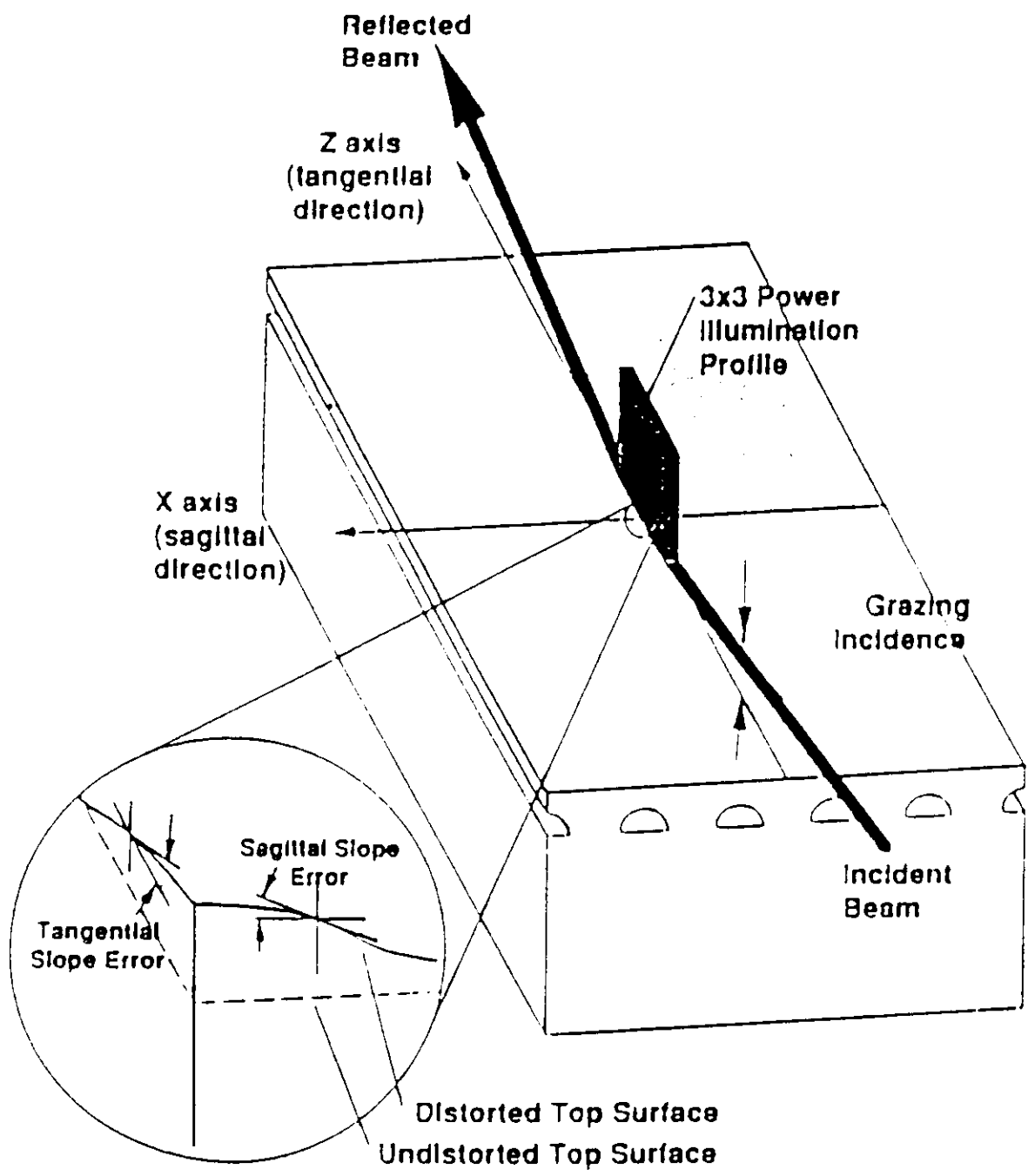
- X-ray mirror

- *working condition:*
  - . total external reflection
- *optical function:*
  - . deflecting/focusing
  - . filtering
- *thermal load:*
  - . low glancing angle ==> large spread-out
- *required slope error or figure tolerance:*
  - .  $1 \div 2 \mu\text{rad}$

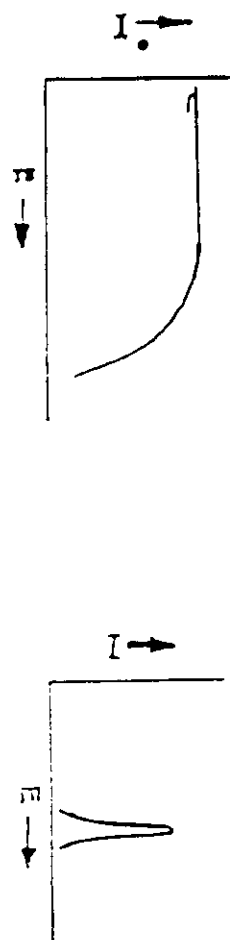
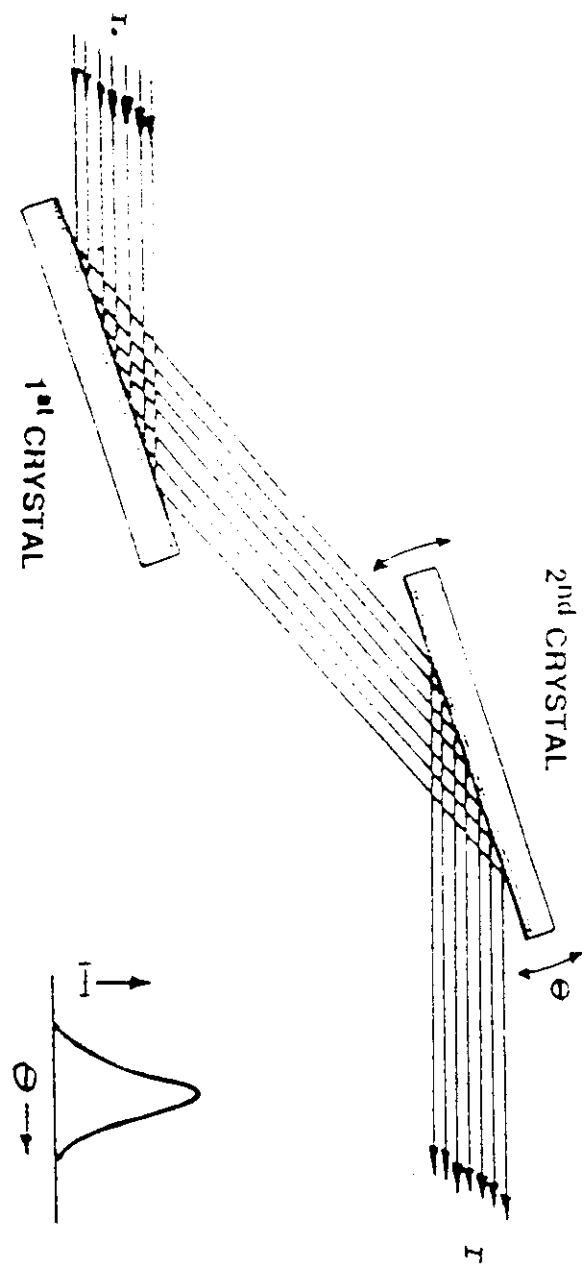
- Perfect single crystal

- *working condition:*
  - . Bragg diffraction
- *optical function:*
  - . monochromatizing
- *thermal load:*
  - . smaller incident angles ==> higher power density
- *allowable thermal distortion of the atomic planes:*
  - . within Darwin widths

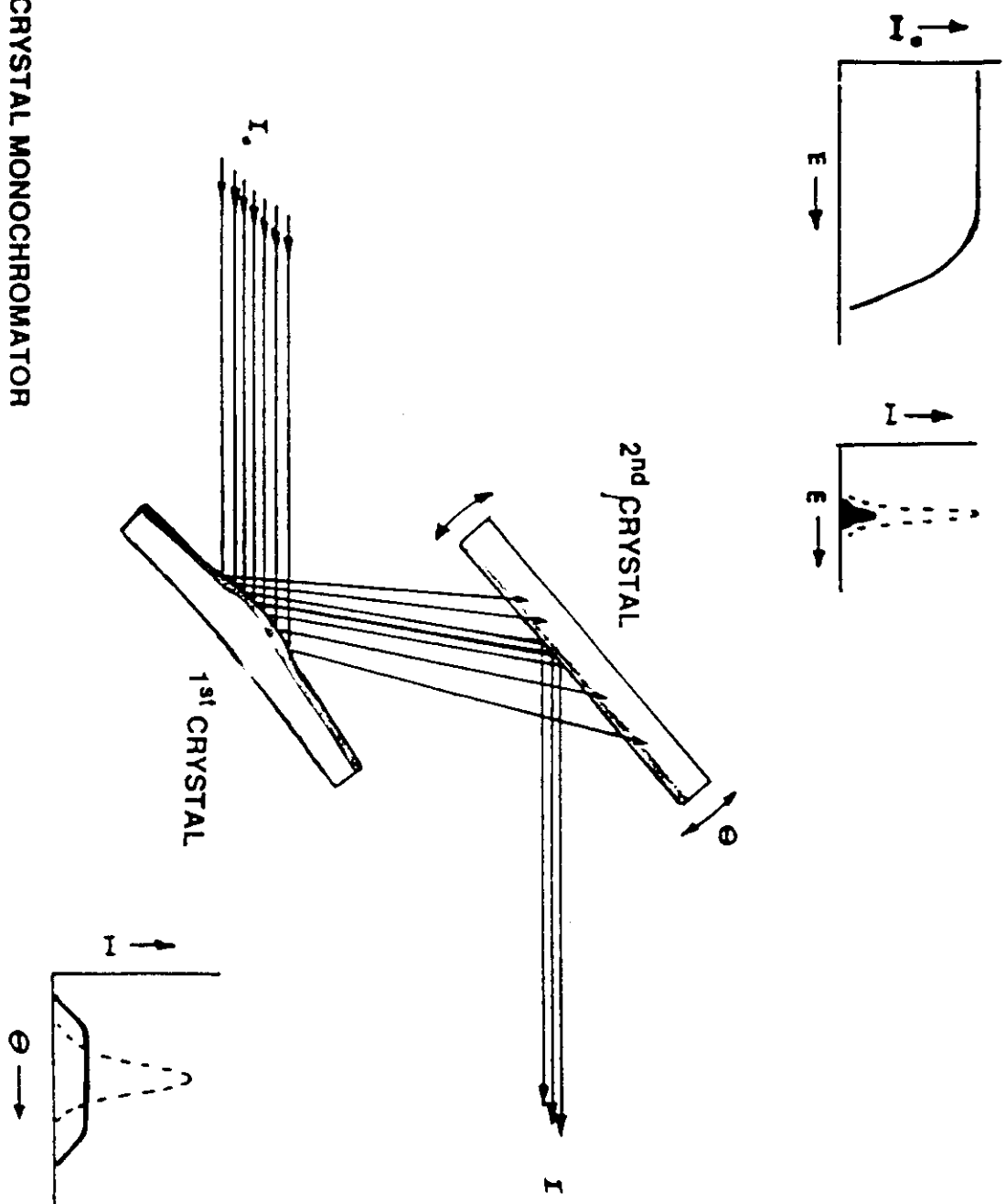


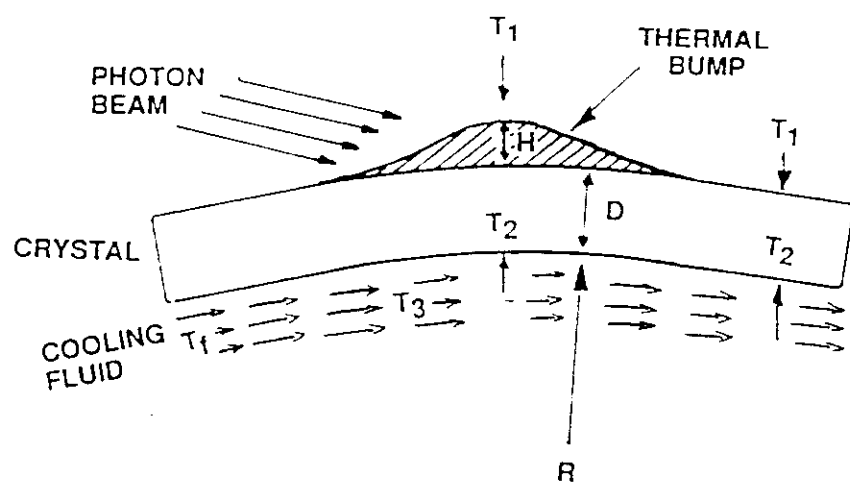


2 CRYSTAL MONOCHROMATOR



2 CRYSTAL MONOCHROMATOR





Schematic drawing of a silicon crystal showing distortion resulting from the high heat load of an intense x-ray synchrotron beam.

# Thermal Distortions

## Scheme:

- a) the crystal is a plate of uniform thickness
- b) no spreading of the heat parallel to the surface
- c) backside cooling

- $T_1 = \Delta T_{12} + \Delta T_{23} + \Delta T_3 + T_f$
- $\Delta T_{12} = T_1 - T_2 = \frac{DQ}{k}$
- $\Delta T_{23} = T_2 - T_3 = \frac{Q}{h}$
- $\Delta T_3 = T_3 - T_f = \frac{1}{H_c V_a C_V} \int Q(x) dx$
- $\Delta T_1 = T_1 - T_f$

$-T_1$	temperature of the diffraction surface [°C]
$-T_2$	temperature of the crystal in contact with the fluid [°C]
$-T_3$	average temperature of the fluid [°C]
$-T_f$	bulk temperature of the fluid [°C]
$-D$	thickness of the crystal above the cooling channel [cm]
$-Q$	heat flux per unit area [W·cm <sup>-2</sup> ]
$-k$	thermal conductivity of the crystal [W·cm <sup>-1</sup> ·°C <sup>-1</sup> ]
$-h$	film coefficient [W·cm <sup>-2</sup> ·°C <sup>-1</sup> ]
$-C_V$	volume specific heat of the fluid [J·cm <sup>-3</sup> ]
$-H_c$	depth of the cooling channel [cm]
$-V_a$	average velocity of the fluid [cm·sec <sup>-1</sup> ]

# Three different components of distortion

## 1. bending

caused by the thermal expansion of the crystal in the direction parallel to the surface, due to the thermal variation along the depth of the crystal.  
The radius  $R$  of the bowing is:

$$R = \frac{D}{\alpha \Delta T_{12}} = \frac{k}{\alpha Q}$$

$\alpha$  [ $^{\circ}\text{C}^{-1}$ ] thermal expansion coefficient.

*Remarks:*

- $R$  is proportional to figure of merit  $k/\alpha$ .
- $R$  does not depend on crystal thickness  $D$ .
- $R$  is independent on the cooling efficiency.
- The thickness of the crystal below the cooling channel stiffens the crystal and reduces the bowing.

Approximately the change in the angle of the surface is given by:

$$\Delta\Theta_s = \frac{\alpha}{k} Q \Delta L = \frac{\Delta L}{R}$$

$\Delta L$  distance along the bowed surface

*Example:*

Silicon Crystal:

$$\alpha = 2.5 \cdot 10^{-6} \text{ } ^\circ\text{C}^{-1}; k = 1.5 \text{ W} \cdot \text{cm}^{-1} \cdot ^\circ\text{C}^{-1};$$

- heat flux  $Q = 100 \text{ W} \cdot \text{cm}^{-2}$

$$R = 6 \cdot 10^3 \text{ cm}$$

and the "bowing distortion" for unit length is:

$$\Delta\Theta_s = 34 \text{ arcsec} \cdot \text{cm}^{-1}$$

## 2. bump

caused by the thermal expansion of the crystal in the direction perpendicular to the surface, due to the thermal variation along directions parallel to crystal surface. The height  $H$  of the bump is given by:

$$H = \alpha D \left( \frac{\Delta T_{12}}{2} + \Delta T_{23} + \Delta T_3 \right)$$

that is:

$$H = \alpha \left( \frac{Q D^2}{2k} + \frac{Q D}{h} + \Delta T_3 D \right)$$

*Remarks:*

- $H$  is proportional to the expansion coefficient  $\alpha$ .
- For large crystal thickness the first term dominates and  $H$  depends mostly on value of  $D$ .
- For small value of  $D$  the second term dominates and  $H$  is inversely proportional to  $h$  that is related with the cooling efficiency of the fluid.
- For reducing the bump:
  - ====> improvement of the figure of merit  $k/\alpha$ .
  - ====> thin crystals
  - ====> high cooling efficiency

Approximately the shape of the bump can be considered Gaussian, then the maximum slope error is given by:

$$\Delta\theta_{max} = \pm 1.4 \frac{H}{FWHM}$$

$FWHM$  depends on the spot size on the crystal

*Example:*

Silicon Crystal:

$$\alpha = 2.5 \cdot 10^{-6} \text{ } ^\circ\text{C}^{-1}; k = 1.5 \text{ W} \cdot \text{cm}^{-1} \cdot ^\circ\text{C}^{-1}; D = 0.2 \text{ cm}; H_c = .25 \text{ cm.}$$

- heat flux  $Q = 100 \text{ W} \cdot \text{cm}^{-2}$ ;  $FWHM = 2 \text{ cm}$ ;  $V_a = 100 \text{ cm} \cdot \text{sec}^{-1}$

- Liquid Gallium ( $C_v = 2.4 \text{ J} \cdot \text{cm}^{-3}$ )

$$\rightarrow h = 5 \text{ W} \cdot \text{cm}^{-2} \cdot ^\circ\text{C}^{-1}$$

$$\rightarrow \Delta T_s = 1.7 \text{ } ^\circ\text{C}$$

$$H = 0.14 \text{ } \mu\text{m}, \quad \Delta\theta_{max} = \pm 2.0 \text{ arcsec}$$

- Water ( $C_v = 4.1 \text{ J} \cdot \text{cm}^{-3}$ )

$$\rightarrow h = 1 \text{ W} \cdot \text{cm}^{-2} \cdot ^\circ\text{C}^{-1}$$

$$\rightarrow \Delta T_s = 0.4 \text{ } ^\circ\text{C}$$

$$H = 0.54 \text{ } \mu\text{m}, \quad \Delta\theta_{max} = \pm 7.8 \text{ arcsec}$$

### 3. variation of the crystal lattice spacing

caused by the thermal gradient along the crystal.  
The variation in the diffraction angle is given by:

$$\Delta\vartheta = \vartheta \alpha \Delta T_1$$

that is:

$$\Delta\vartheta = \vartheta \alpha \left( \frac{DQ}{k} + \frac{Q}{h} + \frac{1}{H_c V_a C_V} \int Q(x) dx \right)$$

*Remarks:*

- The d-spacing variation deforms asymmetrically the rocking curve.
- The angular error  $\Delta\vartheta$  depends on figure of merit  $k/\alpha$  and on the photon energy, as well as on the cooling efficiency.

## Example:

Silicon Crystal:

$\alpha = 2.5 \cdot 10^{-6} \text{ } ^\circ\text{C}^{-1}$ ;  $k = 1.5 \text{ W} \cdot \text{cm}^{-1} \cdot ^\circ\text{C}^{-1}$ ; (1,1,1) planes

$D = 0.2 \text{ cm}$ ;  $H_c = 0.25 \text{ cm}$

- heat flux  $Q = 100 \text{ W} \cdot \text{cm}^{-2}$ ;  $V_a = 100 \text{ cm} \cdot \text{sec}^{-1}$ ;  
 $\vartheta (8 \text{ keV}) = 14.3 \text{ deg}$

- Liquid Gallium ( $C_v = 2.4 \text{ J} \cdot \text{cm}^{-3}$ )

$$\begin{aligned}\rightarrow h &= 5 \text{ W} \cdot \text{cm}^{-2} \cdot ^\circ\text{C}^{-1} \\ \rightarrow \Delta T_s &= 1.7 \text{ } ^\circ\text{C} \\ \rightarrow \Delta T_l &= 35 \text{ } ^\circ\text{C}\end{aligned}$$

$$\Delta\vartheta = \pm 4.6 \text{ arcsec}$$

- Water ( $C_v = 4.1 \text{ J} \cdot \text{cm}^{-3}$ )

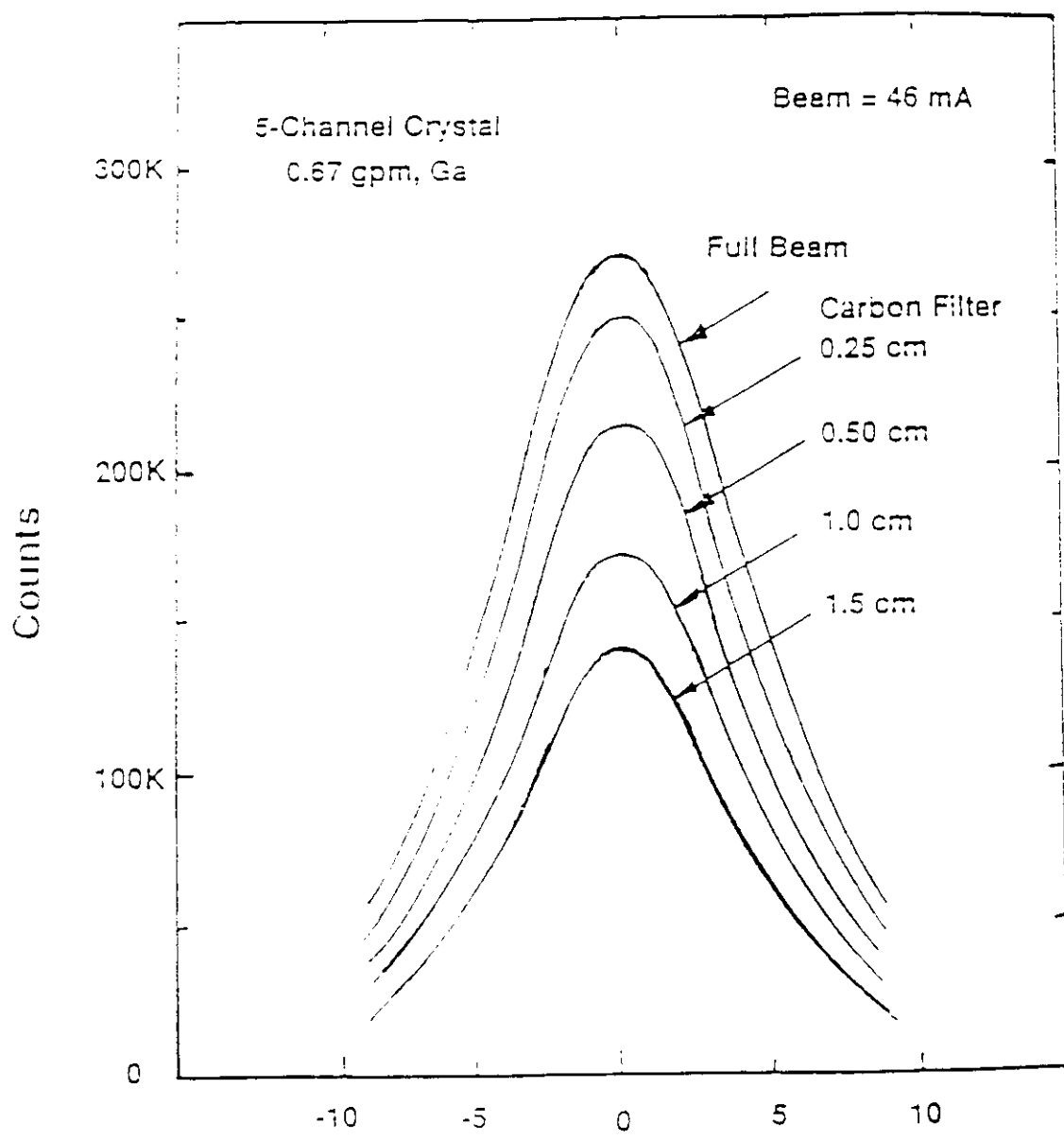
$$\begin{aligned}\rightarrow h &= 1 \text{ W} \cdot \text{cm}^{-2} \cdot ^\circ\text{C}^{-1} \\ \rightarrow \Delta T_s &= 0.4 \text{ } ^\circ\text{C} \\ \rightarrow \Delta T_l &= 114 \text{ } ^\circ\text{C}\end{aligned}$$

$$\Delta\vartheta = \pm 14.7 \text{ arcsec}$$

- These shifts are similar to the widths of the rocking curve of perfect silicon crystal at this energy and cause a mismatch between the first and the second crystal in a double crystal monochromator.

# Minimising heat load problem

- Use of cooled filters:
  - Graphite, Kr gas, Al, Be...
- Improving cooling efficiency:
  - Optimization of cooling geometry
  - Choice of coolant (H<sub>2</sub>O, Ga, N<sub>2</sub>, Propane...)
- Choice of materials:
  - SiC, Diamond...
- Various innovative schemes:
  - Heating from the backside
  - Thin crystals
  - Cryogenic cooling
  - Applying an opposite mechanical momentum



Plot of the counting rate from the diffracted beam of the CHESS two crystal monochromator as a function of the carbon absorber thickness in the beam.

# Cooling geometries

## a) flat plate:

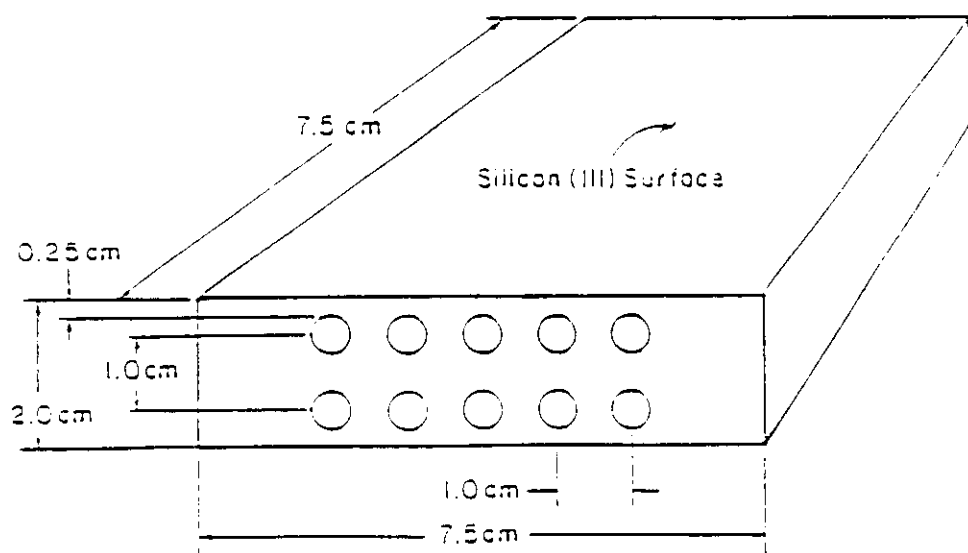
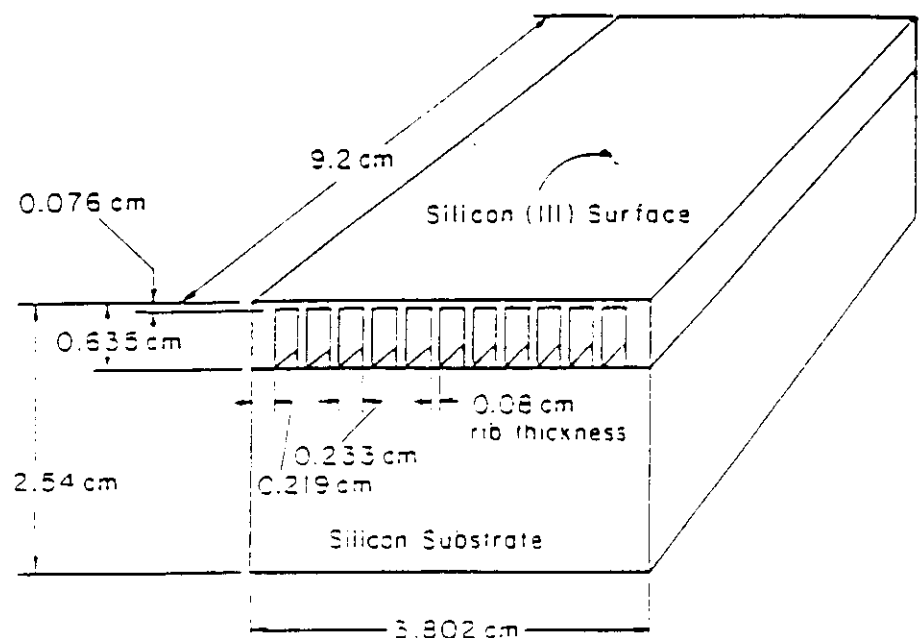
- . side and/or backside (i.e. water cooled cooper block)
- . efficient transfer medium (eutectic alloy InGa, In foil)
- . for small heat loads (few W/cm<sup>2</sup>)
- . simple and more common solution

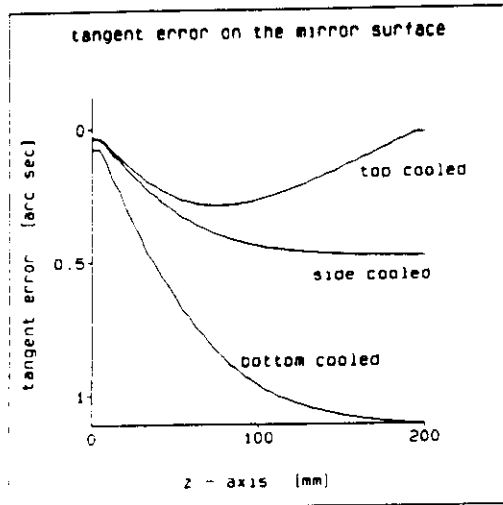
## b) channels:

- . increment of cooling efficiency
- . increment of the effective transfer area
- . thickness under the channels reduces the bowing

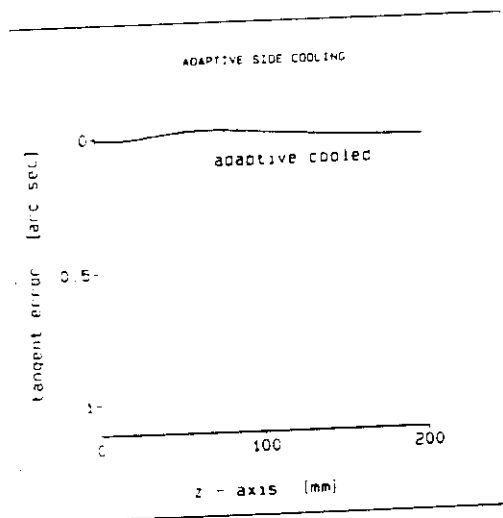
## c) microchannels:

- . features:
  - a) optimization of microchannel/fin widths
  - b) aspect ratio 10:1
  - c) increment of the cooled area by a factor of 10
  - d) laminar water flow

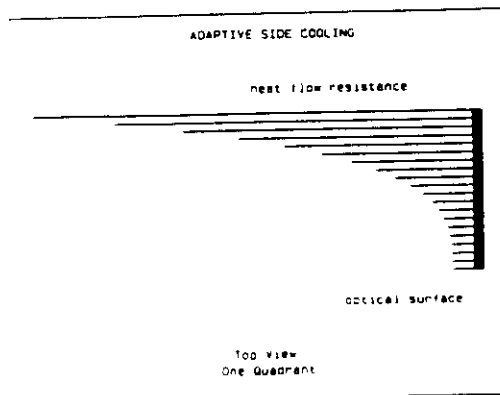




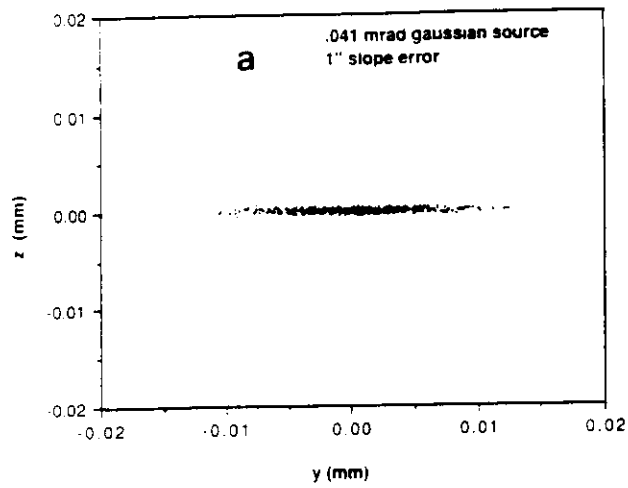
The three test cooling cases. Shown is the tangent error vs position on the mirror surface. Only one half of the mirror is shown.



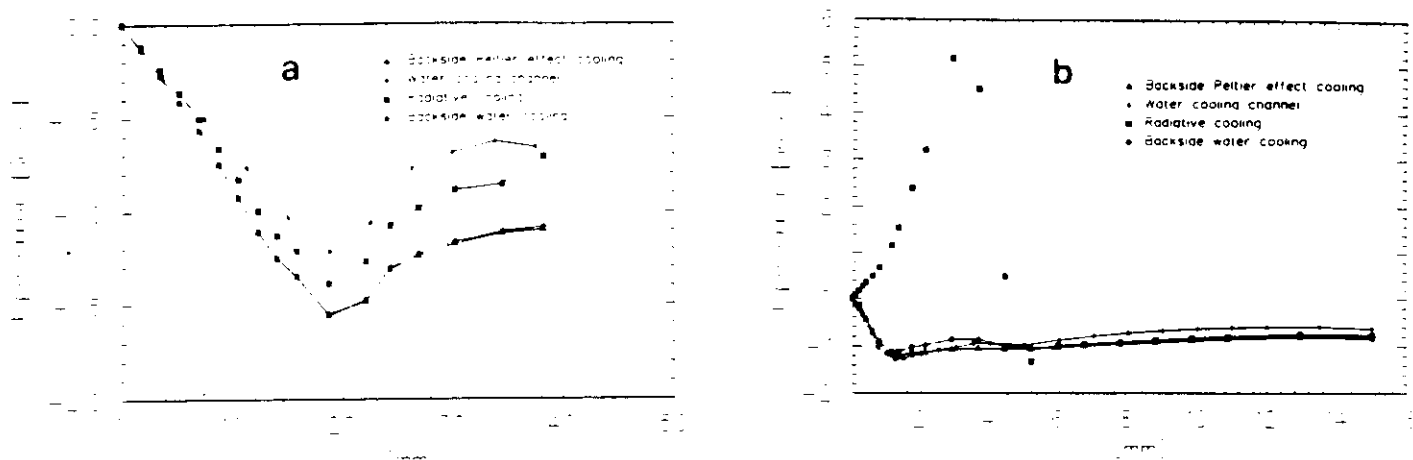
Meridional tangent errors on the adaptively cooled mirror. The tangent errors are much smaller than the 0.1 arcsec rms tangent error and hence do not deteriorate the focusing properties of the mirror.



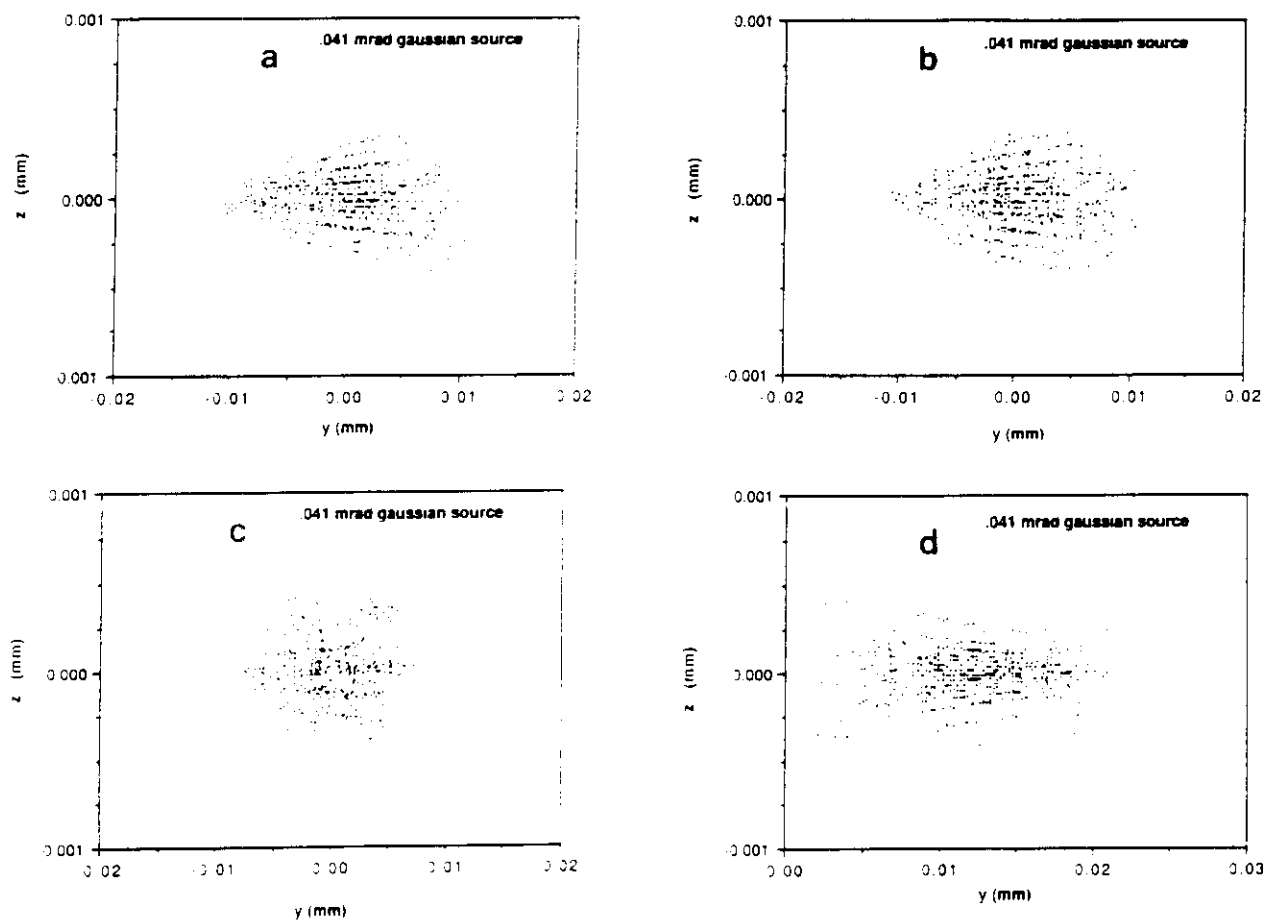
FEM analysis for adaptive side cooling showing the heat flow pattern necessary to produce laminar isotherms parallel to the long sides of the mirror. Note that the lines projecting out from the side of the mirror quadrant are proportional to the resistance to heat flow.



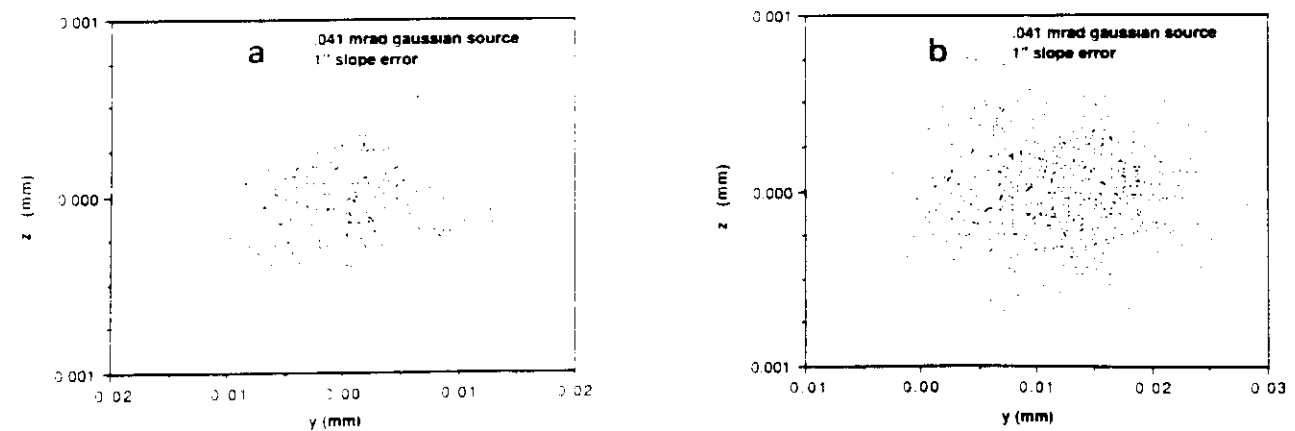
Focal images obtained with 1 arcsec random slope error on mirrors: (a) ellipsoidal mirror



Slope errors on mirror surface for different cooling schemes in (a) tangential direction and (b) sagittal direction.

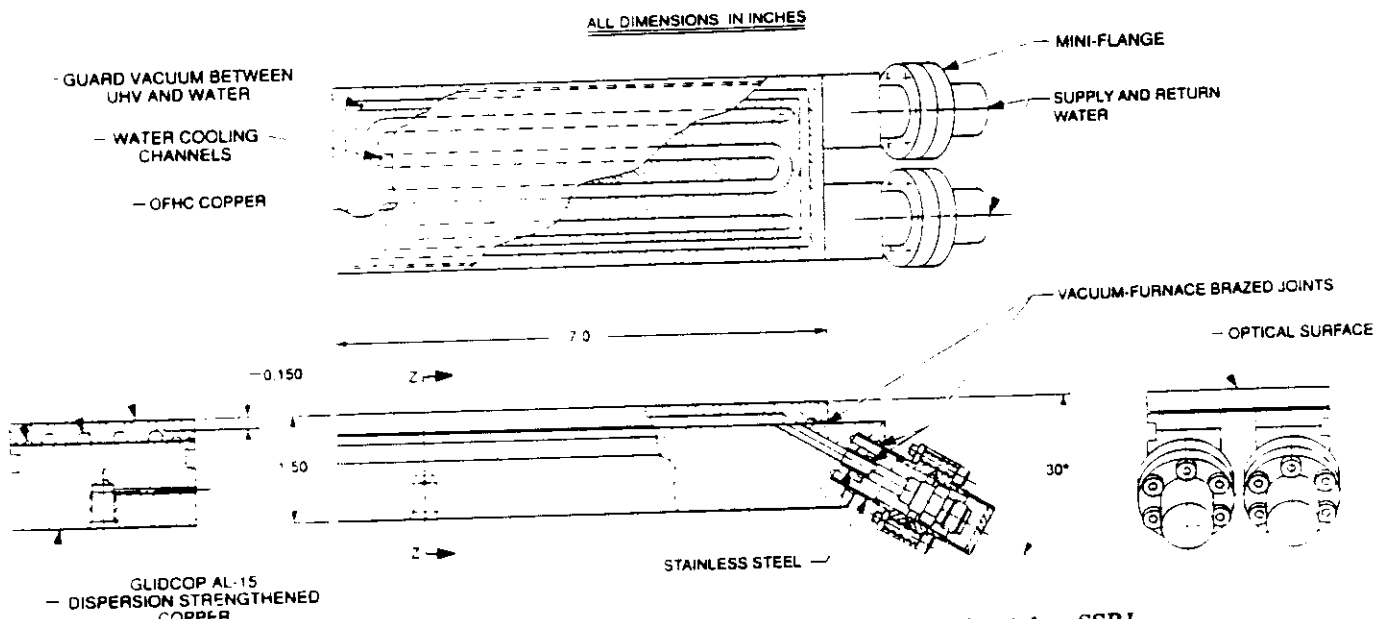


Focal-ray pattern of the ellipsoidal mirror with thermal load only: (a) constant water cooling on back; (b) uniform backside temperature (Peltier effect heat exchanger); (c) water-cooling channel; and (d) radiative cooling.

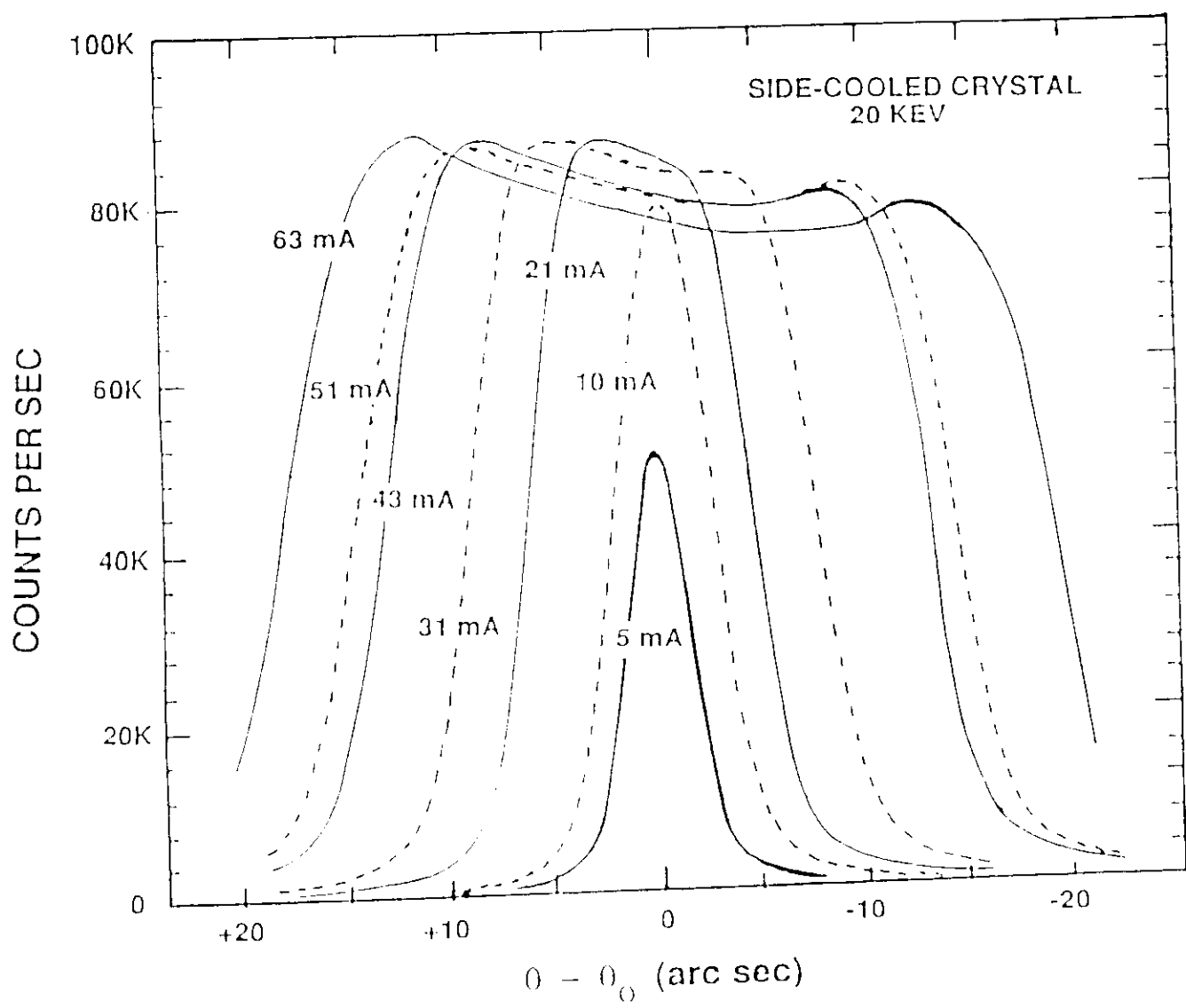


Focal ray pattern of the ellipsoidal mirror with thermal load and 1 arcsec slope error: (a) water-cooling channel; (b) radiative cooling.

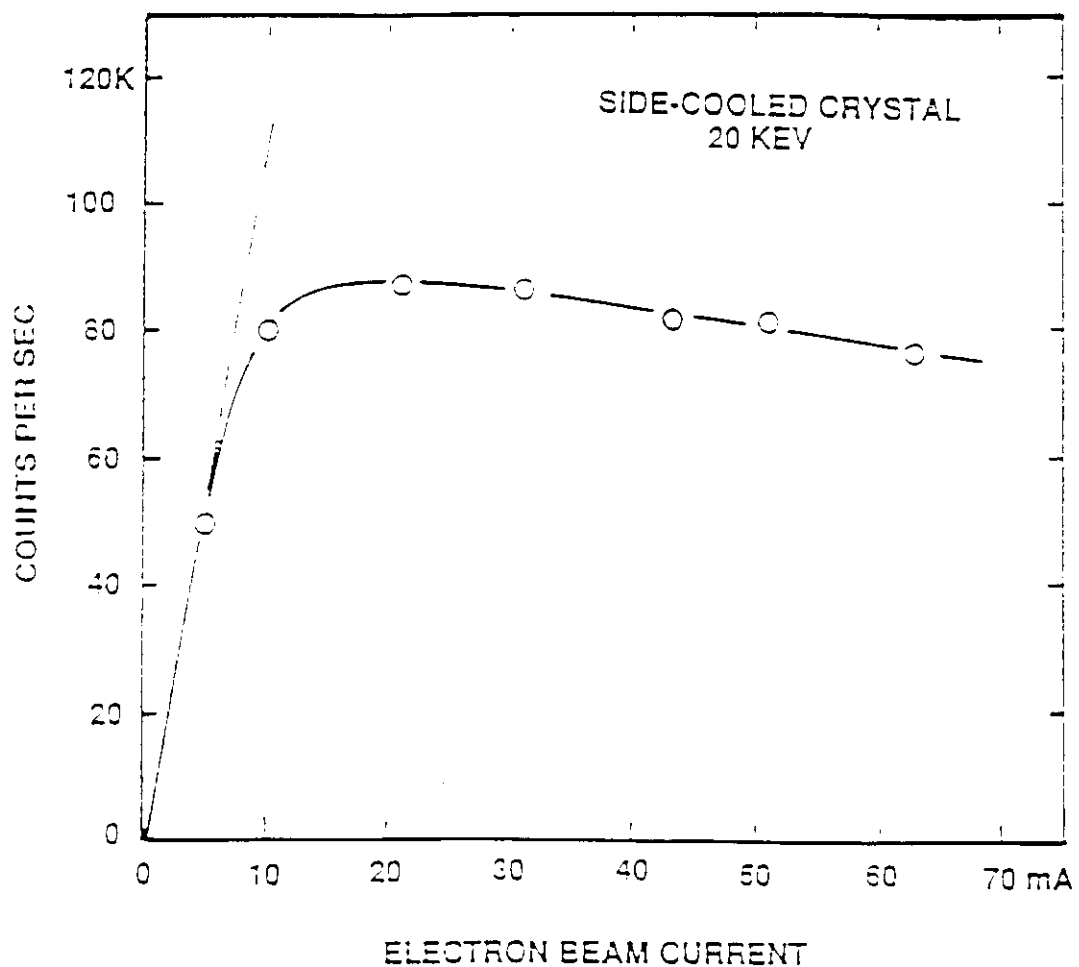
DIFFRACTION GRATING SUBSTRATE  
BRAZE ASSEMBLY



LBL-SGM water cooled grating substrate details for Beam Line 6-1 at SSRL.



Rocking curves for the side-cooled, bottom-cooled crystal for different currents in the storage ring.



Plot of the peak counting rate in the CHESS two crystal monochromator versus electron beam current in the storage ring when the first crystal is the standard side-cooled, bottom cooled silicon (111) crystal.

optimized channels for a fixed pressure drop:

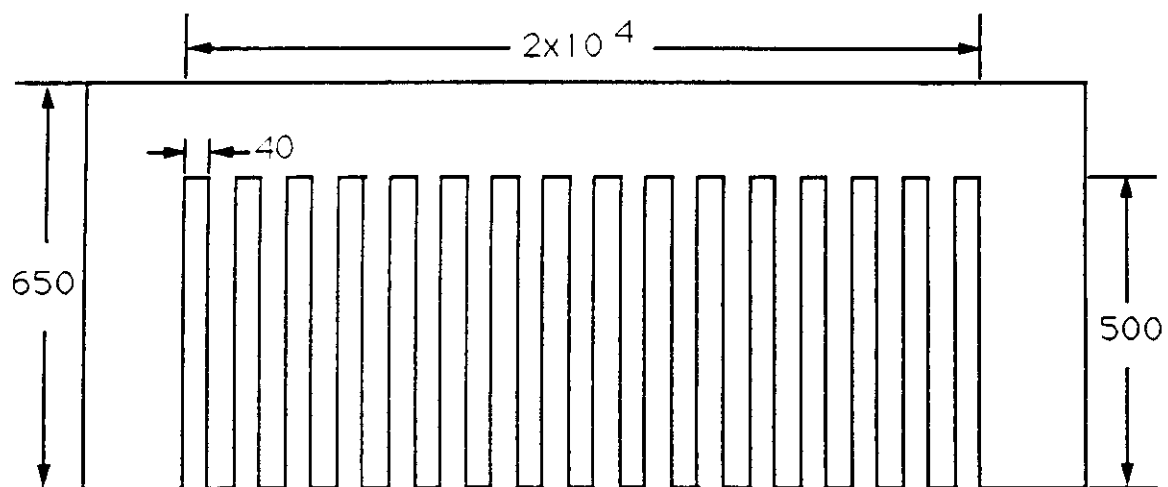
$$\theta_{\text{opt}} = 2.95 \left[ \frac{C_f v D}{K_c \text{Nu} k_w^2 L^2 W^4 C P} \right]^{1/4}$$

$C_f$  = friction coefficient

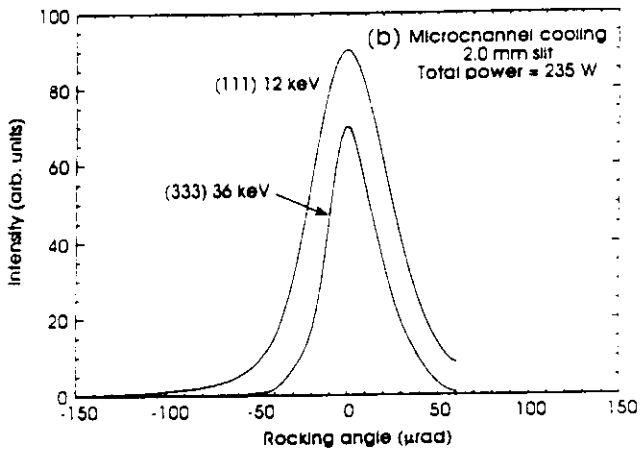
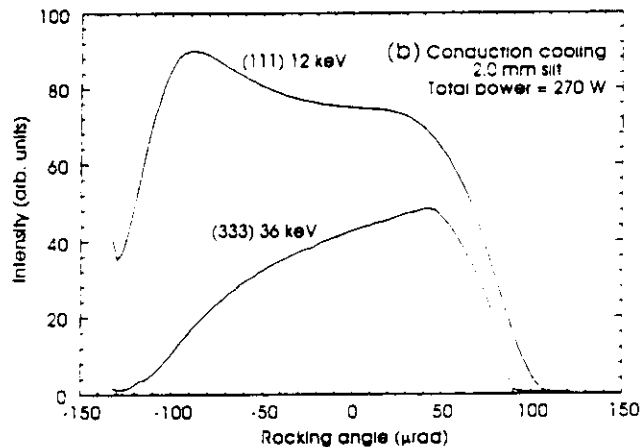
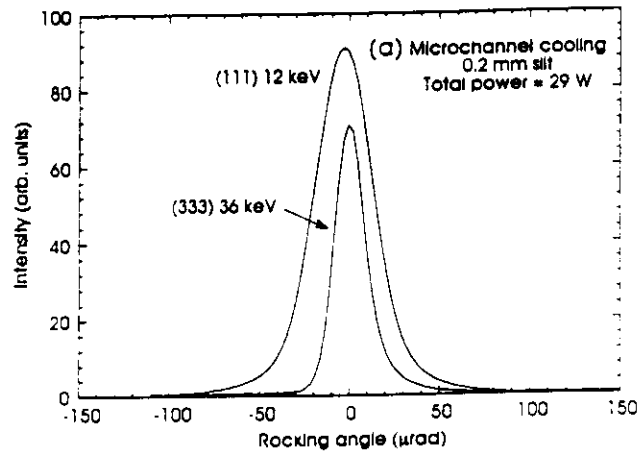
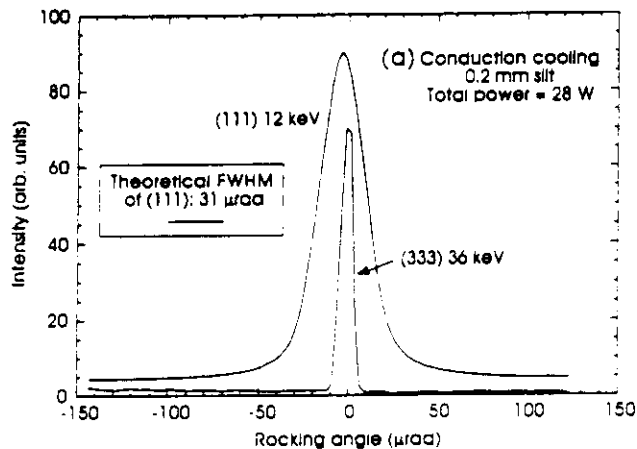
$v$  = coolant velocity

$P$  = pressure drop

optimization applied to a silicon wafer with water cooling:



dimensions =  $\mu\text{m}$



Rocking curves obtained with a crystal cooled by conduction to a water-cooled copper base. The (111) and (333) intensities have been multiplied by different scaling factors. Here (a) shows the low-power results. The (111) 12 keV curve has a full width at half-maximum (FWHM) equal to the theoretical calculation for perfect crystals. The (333) 36 keV curve is slightly broader than the theoretical calculation, which has a FWHM of 2.0  $\mu$ rad. The high-power results are shown in (b). Severe thermal strain caused grossly deformed rocking curves. Under these conditions, the observed temperature rise of the hot spot on the crystal was 65 °C.

Rocking curves obtained with a microchannel-cooled crystal. Once again, the (111) and (333) intensity values have been multiplied by different scaling factors. The low-power (111) curve in (a) is only slightly broader than the perfect-crystal calculation, though the (333) curve shows the presence of a small amount of permanent strain in the crystal. Under high-power conditions (b), only a small amount of heat-induced strain is indicated. The temperature rise of the hot spot on the crystal under high-power loading was about 5 °C.

# Liquid Gallium cooling

## Favourable properties

- High thermal conductivity
- High specific heats
- Large range of working temperatures
- Low vapour pressure
- Room temperature melting point

## Drawbacks

- High reactivity with other metals (but not with silicon and stainless steel  $T < 400$  °C)
- Liquid metal pump<sup>(\*)</sup>
  - high pressure
  - moderate flow rate

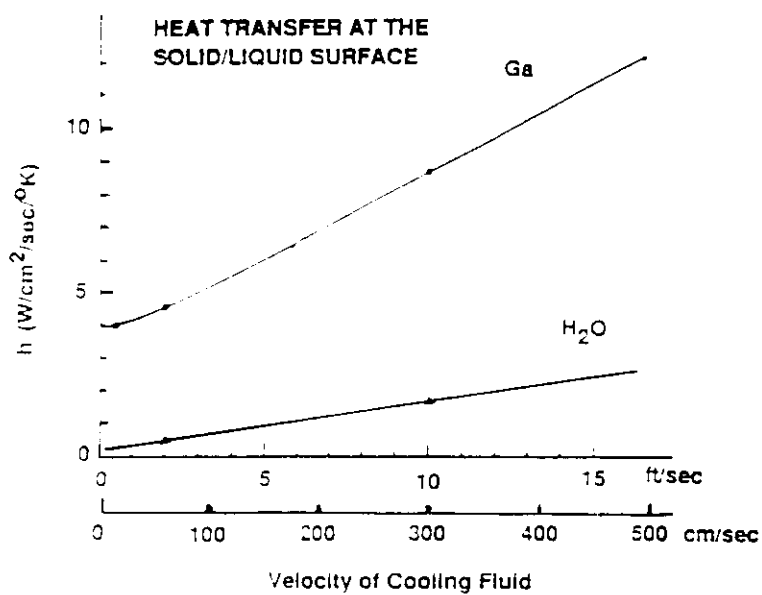
(\*) Film coefficient for liquid metal flow (Baker and Tessier):

$$h = A_1 \frac{k}{d} + A_2 \frac{k^{0.6}}{d^{0.2}} \frac{C_V^{0.4}}{\nu^{0.8}} V_a^{0.8}$$

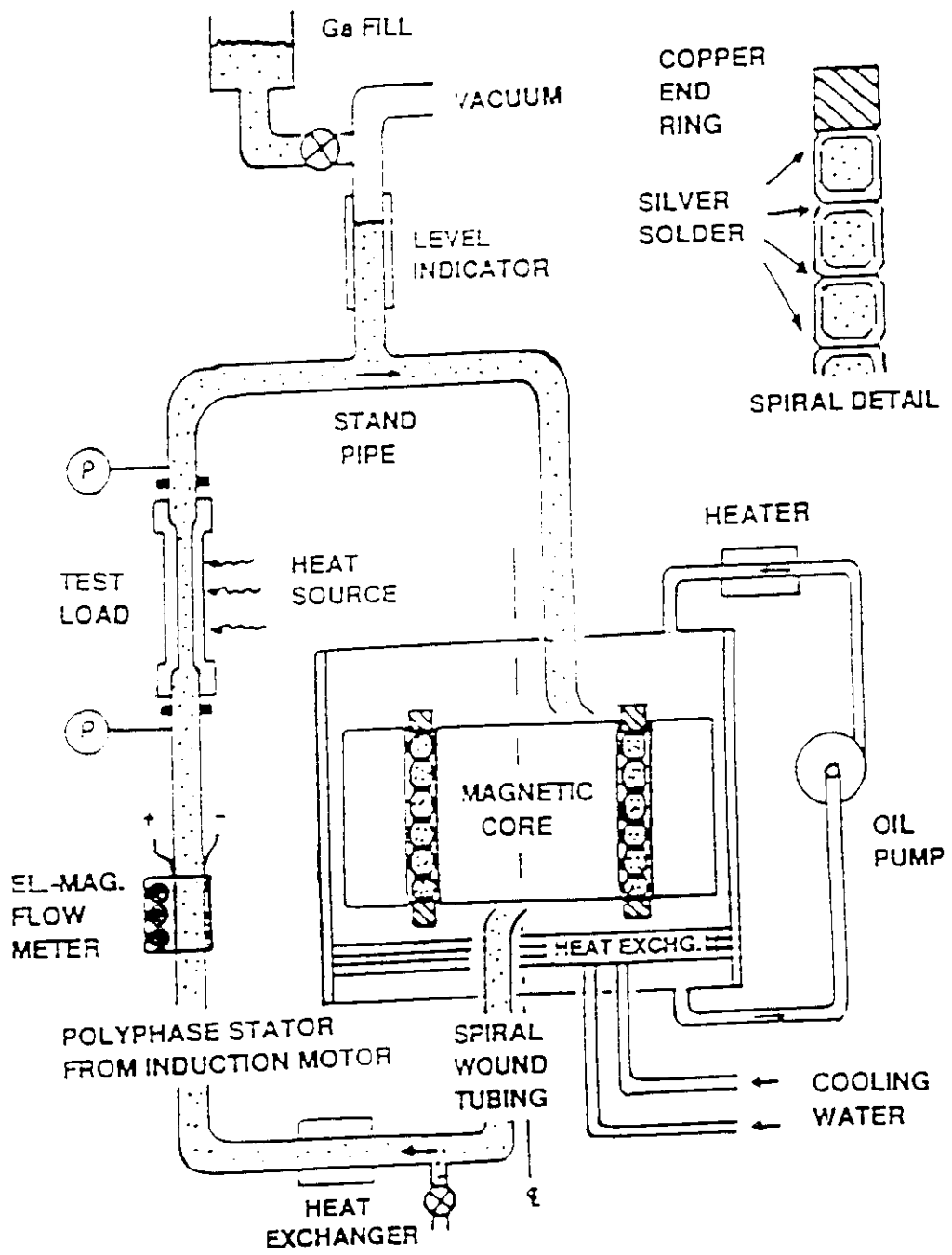
$k$  thermal conductivity;  $d$  hydraulic diameter;  $\nu$  kinetic viscosity;  $C_V$  volume specific heat;  $V_a$  fluid velocity,  $A_1, A_2$  constants with values near 1 (empirically determined).

# Properties of cooling fluids

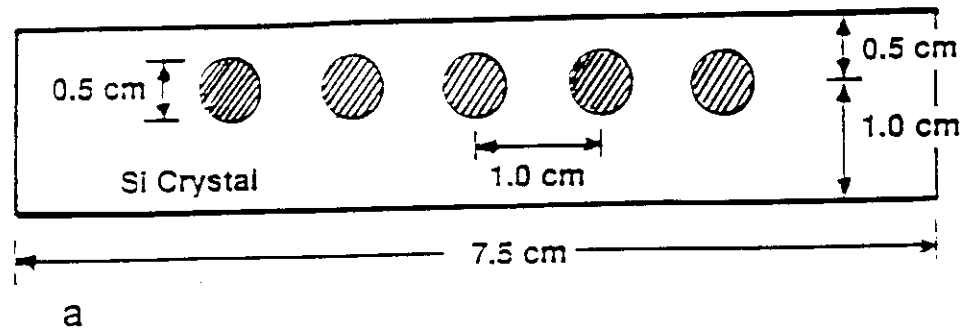
Coolant	M.P. [°C]	B.P. [°C]	V.P. [mm Hg]	$k$ [W·cm <sup>-1</sup> ·K <sup>-1</sup> ]	$C_V$ [J·cm <sup>3</sup> ]	$\nu$ [p·g <sup>-1</sup> ]	$\frac{k^{0.6} C_V^{0.4}}{\nu^{0.8}}$
Ga (50°)	29.8	2071	<10 <sup>-14</sup>	0.33	2.4	0.0026	90.0
H <sub>2</sub> O (20°)	0.0	100	0.17	0.006	4.12	0.0100	5.34
N <sub>2</sub> (-170°)	-210	-196	7.5 10 <sup>3</sup>	0.0014	1.6	0.0021	4.57
C <sub>3</sub> H <sub>8</sub> (-170°)	-187	-42	3.1 10 <sup>-3</sup>	0.0020	1.4	0.0075	1.38



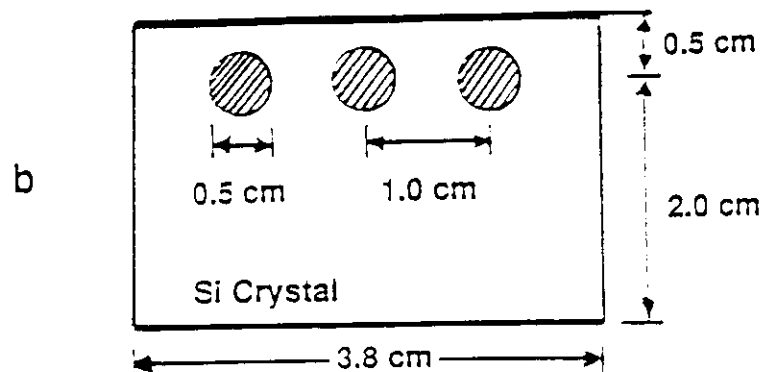
Plot of  $h$ , the heat transfer coefficient, for liquid Ga (upper curve) and for water (lower curve) as a function of cooling-fluid flow rate in an 0.5-cm-diameter channel.



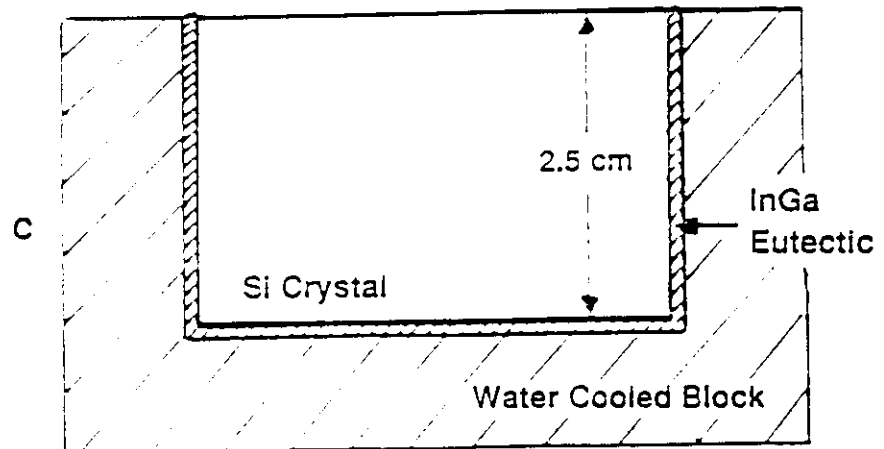
Schematic drawing of the gallium pump.



a

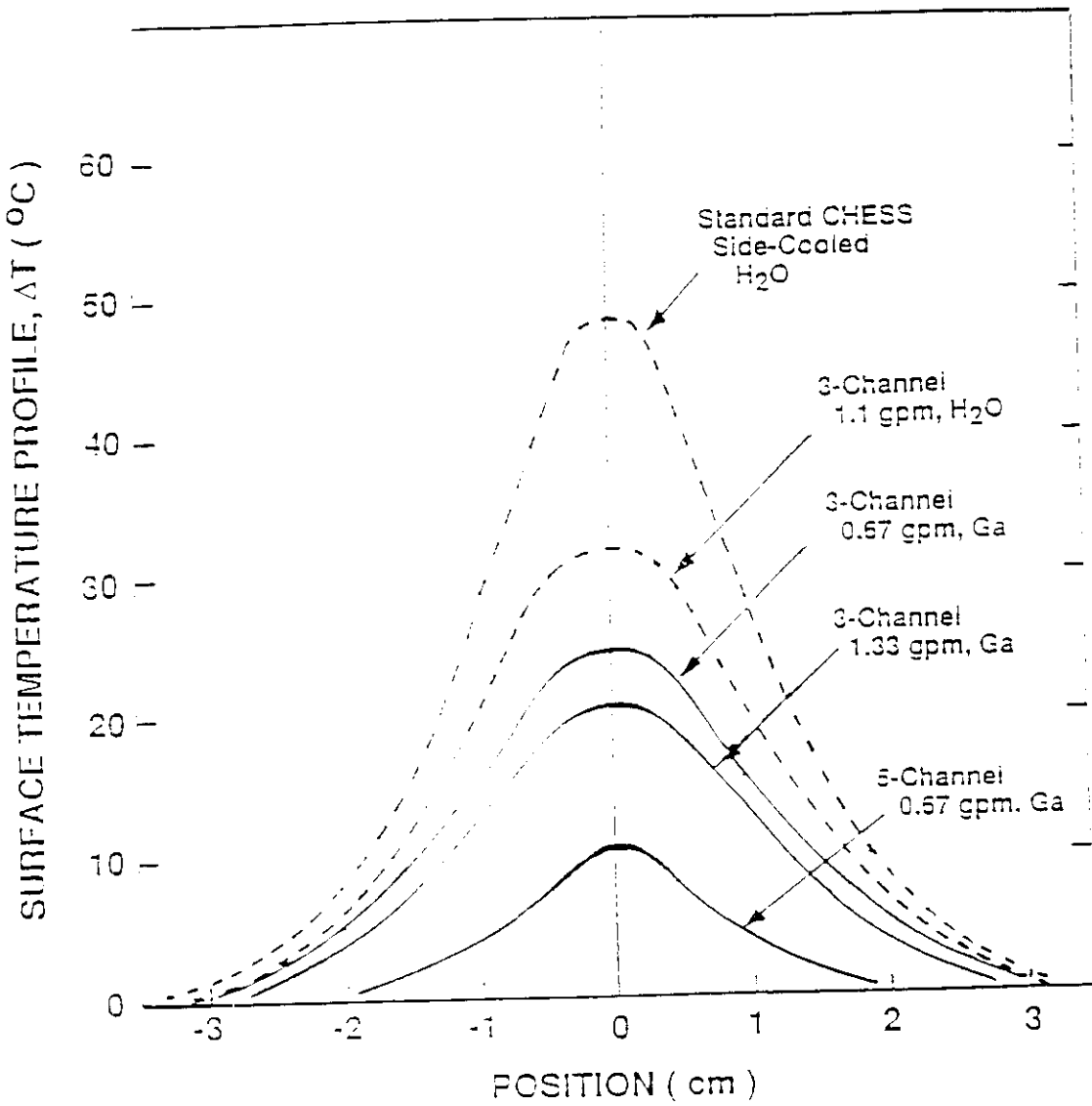


b

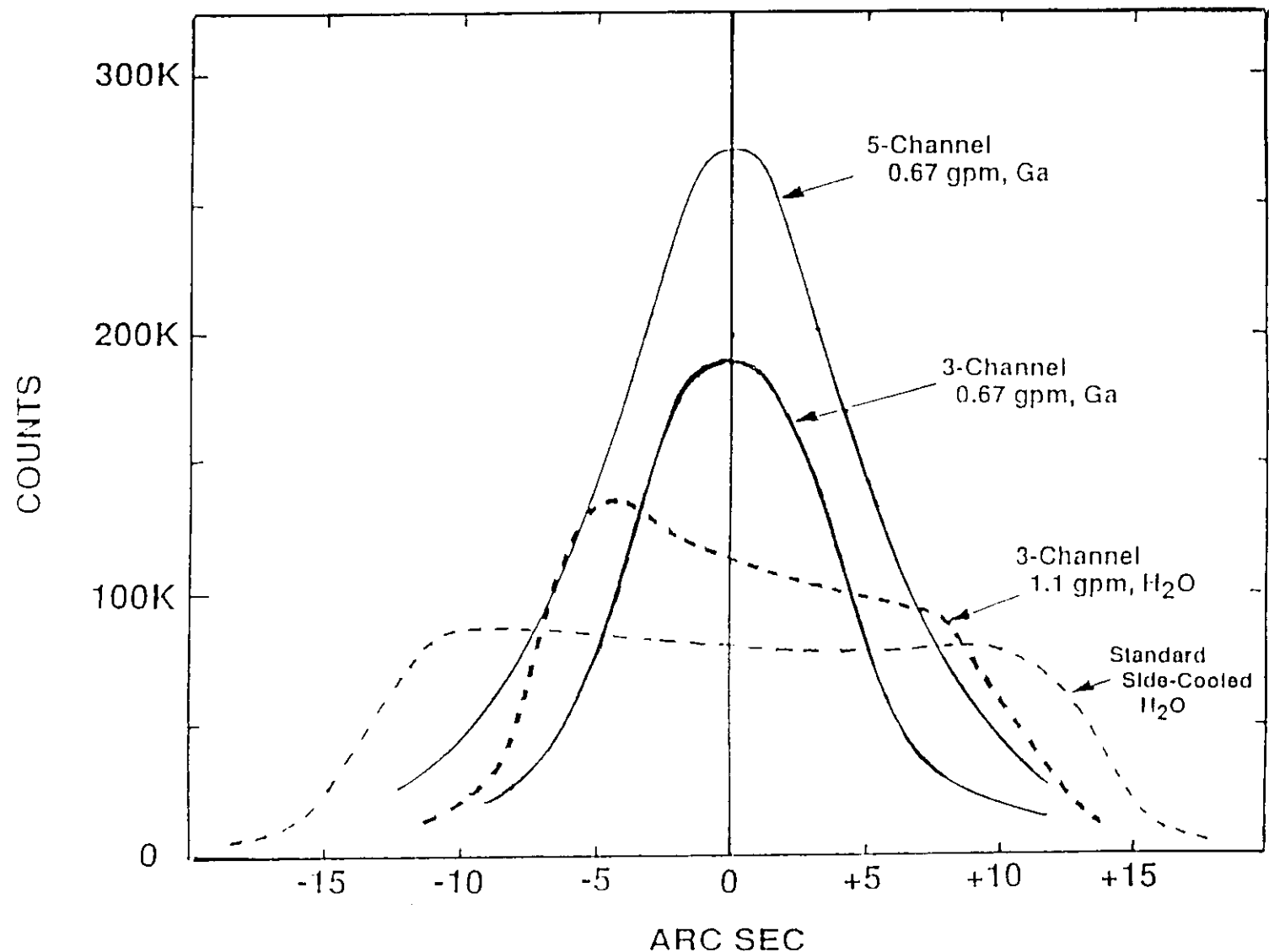


c

Drawings of the cross sections of the three cooled silicon crystals used in the wiggler experiments.

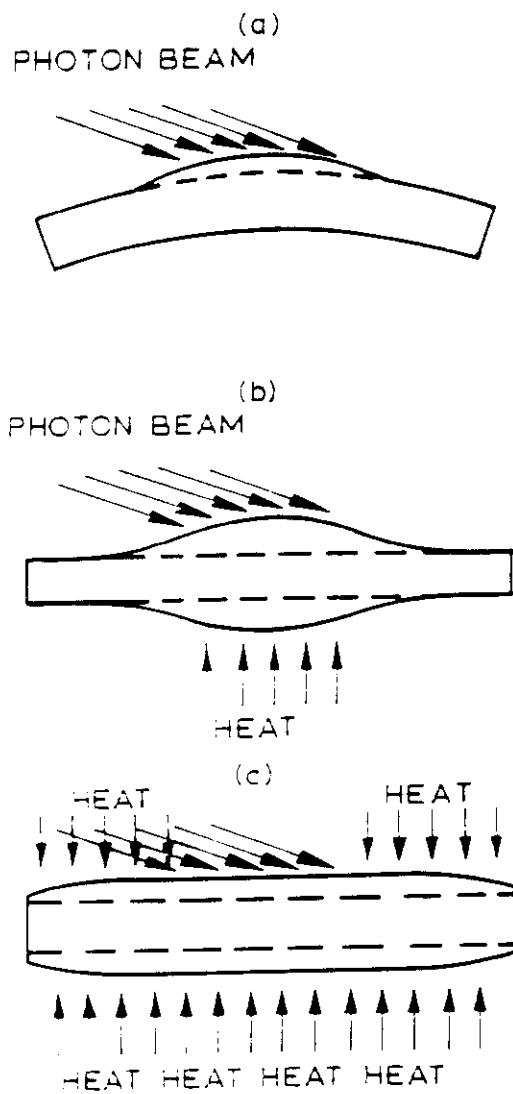


Plot of the surface temperature profile in the direction of the beam for the three different cooled silicon crystals used in the wiggler experiments.



Plot of the rocking curves obtained with the three different silicon crystals in the wiggler experiments ( photon energy = 20 keV, electron current = 46 mA).

# Heating the crystal



Distortion in the crystal surface with large heat loads and possible solutions. (a) Absorbed photon beam "warps" crystal; (b) with backside auxiliary heating, the bowing can be minimized; (c) best solution, add heat to both the front and backsides to unstress the crystal (Smither et al. 1988).

# Cryogenic Cooling

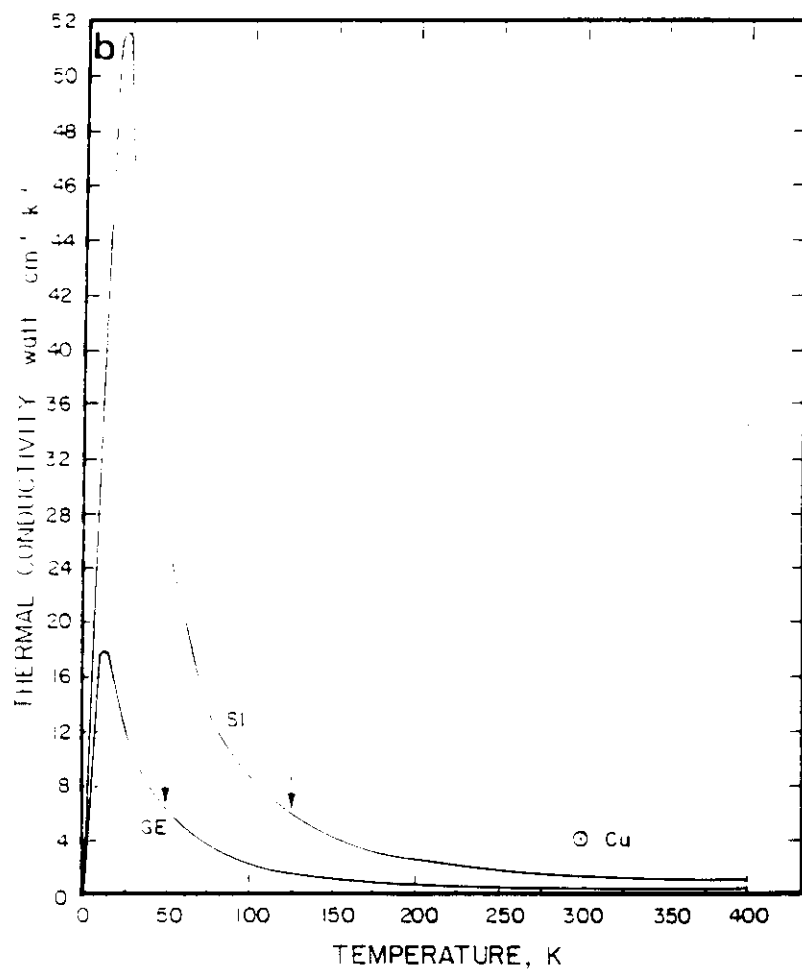
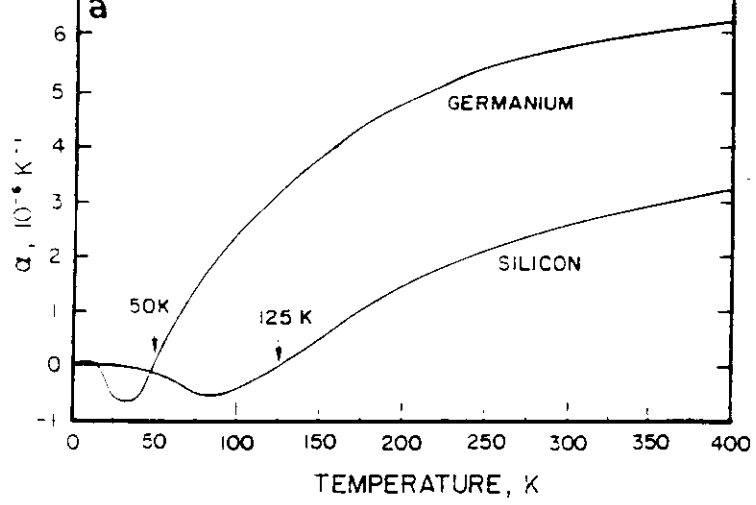
## Properties of some crystals (Si, Ge, etc.)

- Thermal conductivity  $k$  increases when the temperature decreases (up to few tens of K degrees).  
**==> reduction of  $\Delta T$**
- Thermal expansion coefficient  $\alpha$  decreases when the temperature decreases. It goes to 0 at absolute zero and again at 125 K for Si and 50 K for Ge. Between these temperatures  $\alpha$  is negative.  
**==> reduction of d-spacing non uniformity**

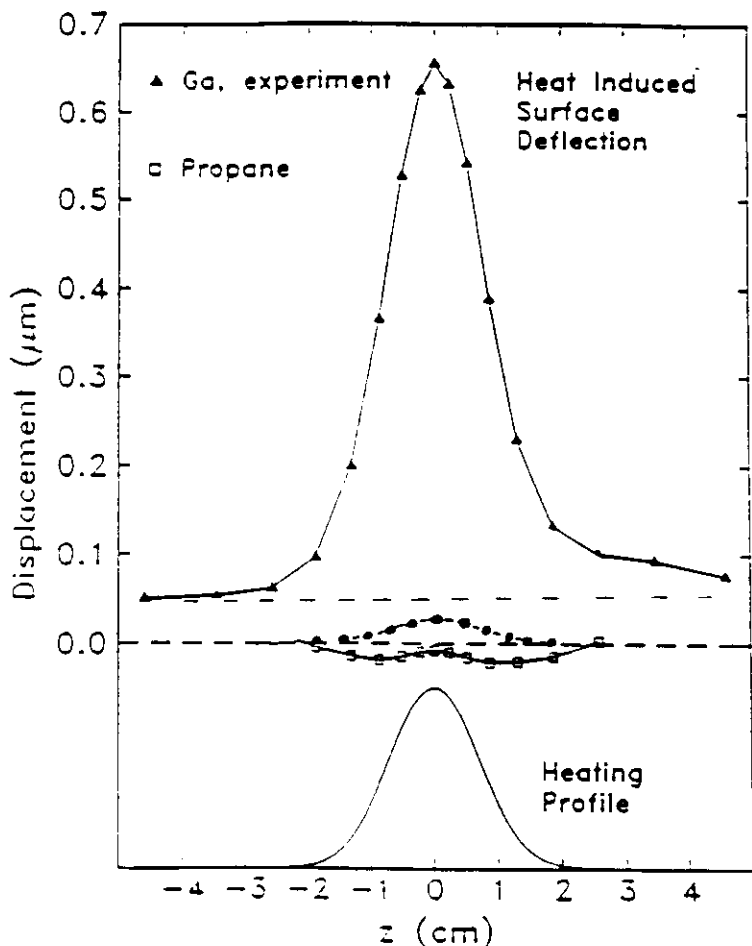
For cooling a Si crystal the fluid must have the following properties:

- liquid phase between 80 and 120 K
- good cooling characteristics
- non-toxic, non-flammable

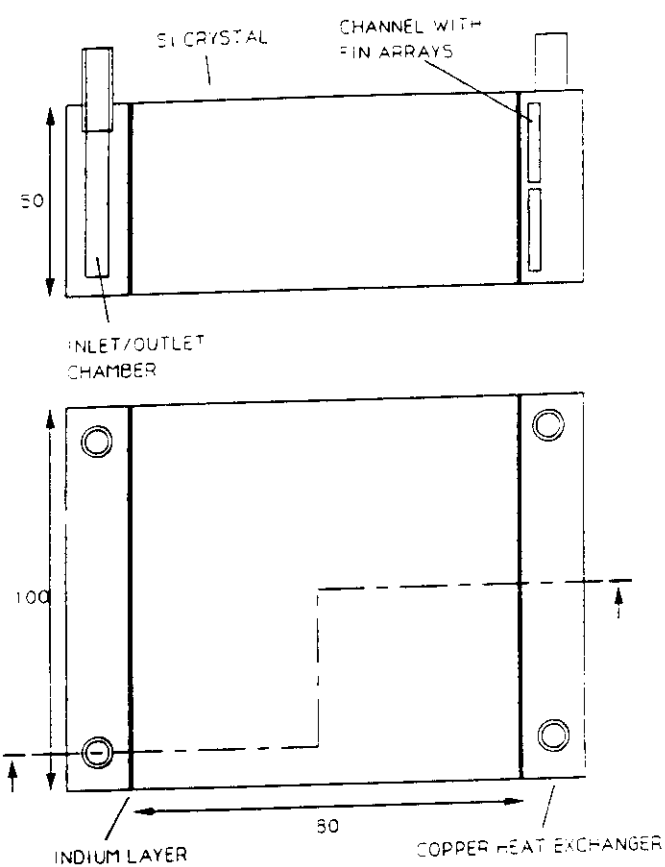
**==> good choice liquid  $N_2$**



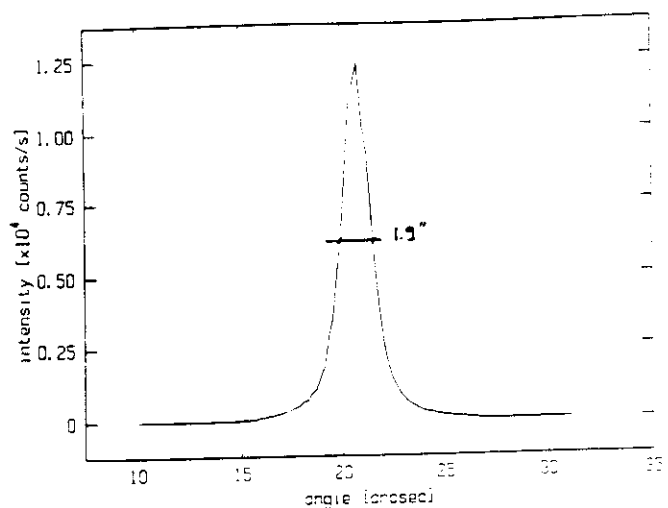
Thermophysical properties of undoped silicon and germanium. (a) Coefficient of thermal expansion goes to zero at 0 and again at 50 K (Ge) and 125 K (Si). (b) Thermal conductivity is greatly improved by operation at low temperatures (Bilderback 1986).



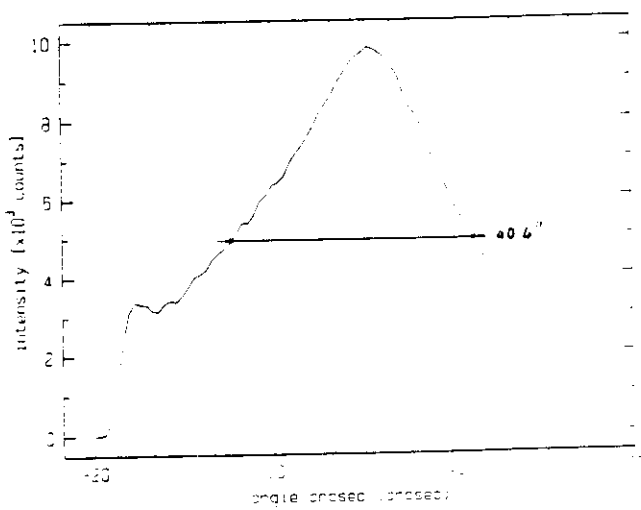
Calculated surface displacement (vertical) of the slotted crystal in the ANL, CHESS undulator beam for experimental conditions in the undulator test with liquid-gallium cooling (triangles), liquid propane (squares) and the limit for either liquid-gallium or water cooling (circles).



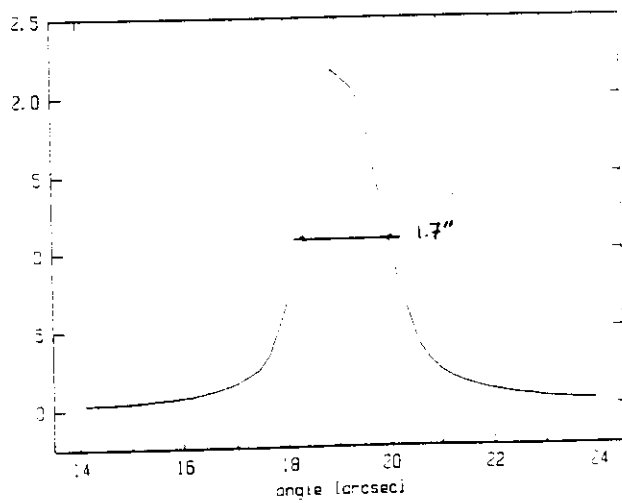
Schematic drawing of the side cooled silicon crystal (fin arrays not shown for simplification).



Intensity vs angle (arcsec). Rocking curve of the side cooled Si crystal. *Crystal temperature: 300 K; absorbed power: 3.8 W.* The measured FWHM is 1.9 in.



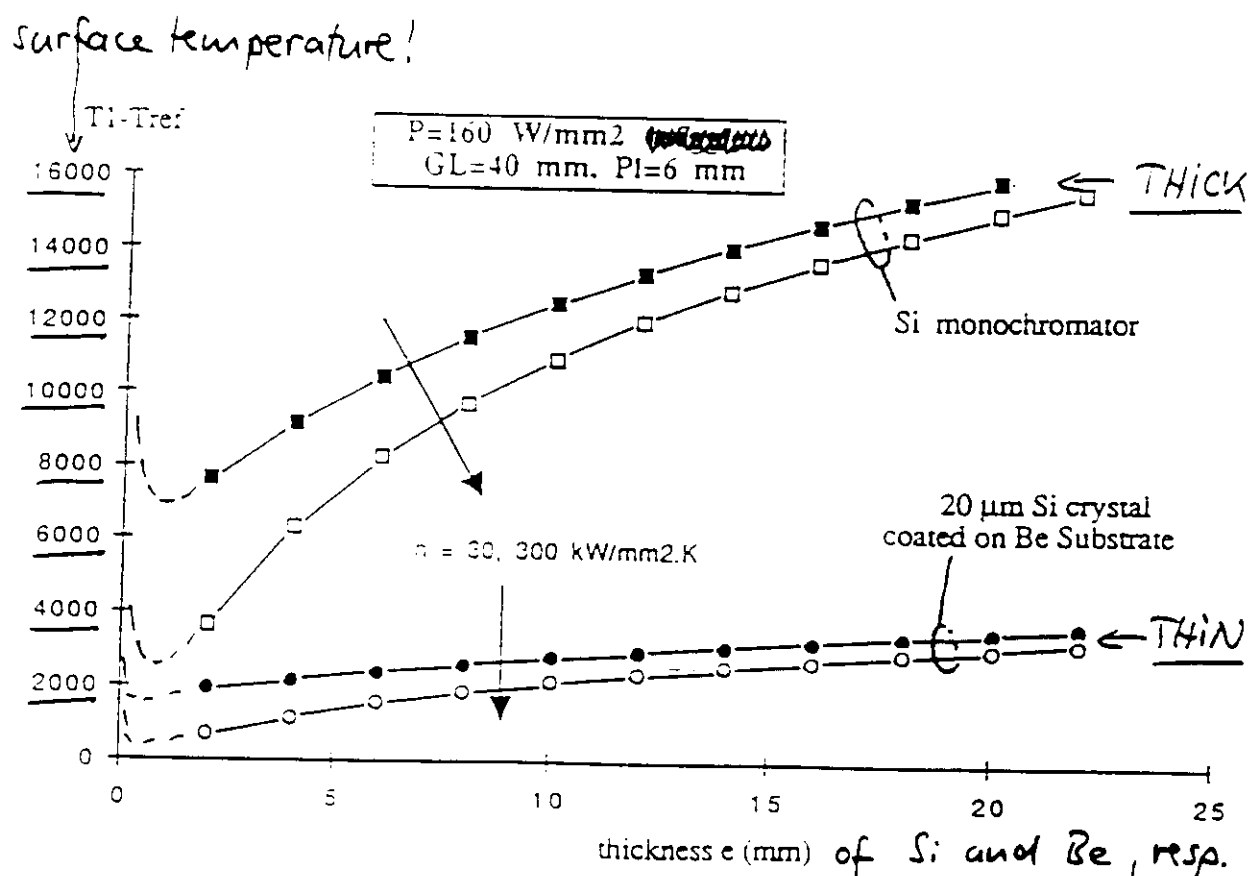
Intensity vs angle (arcsec). Rocking curve of the side cooled Si crystal. *Crystal temperature: 300 K; absorbed power: 60 W.* The measured FWHM is 40.4 in.

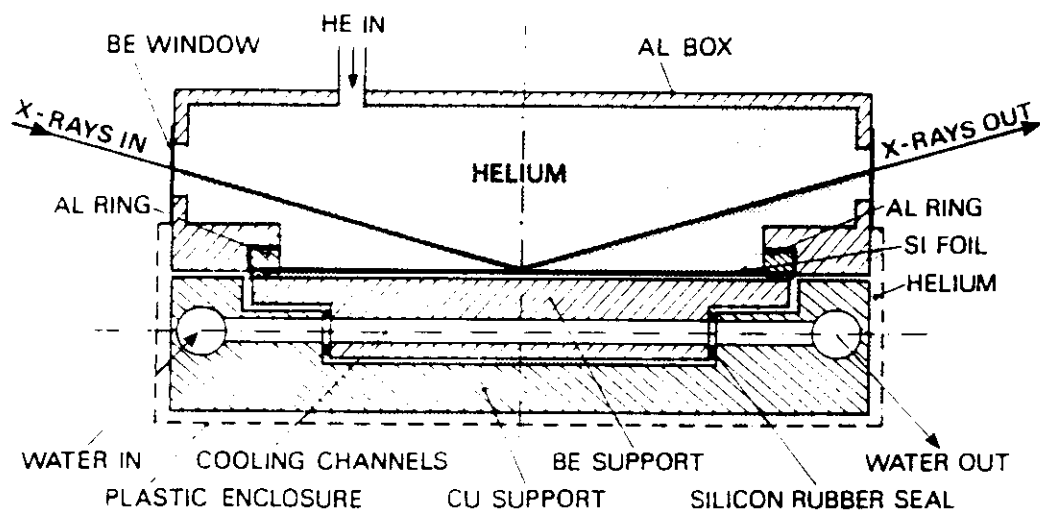


Intensity vs angle (arcsec). Rocking curve of the side cooled Si crystal. *Crystal temperature: 85 K; absorbed power: 75 W.* The measured FWHM is 1.7 in.

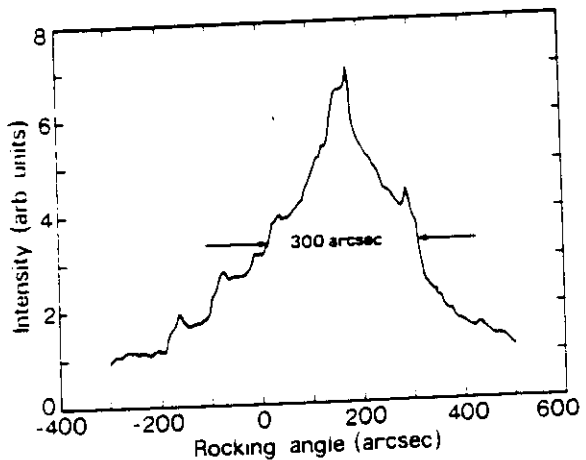
# Thin crystals

- Thermal bending is independent on thickness  $D$ .
- Thermal bump increases as  $D^2$ .
- d-spacing variation increases as  $D$ .
- High of the bump for thin materials depends inversely on  $h$ .

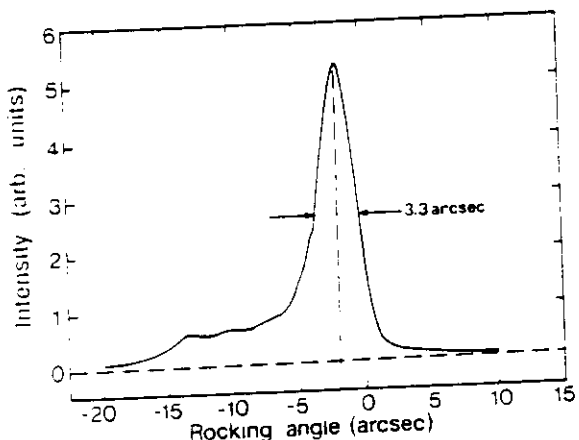




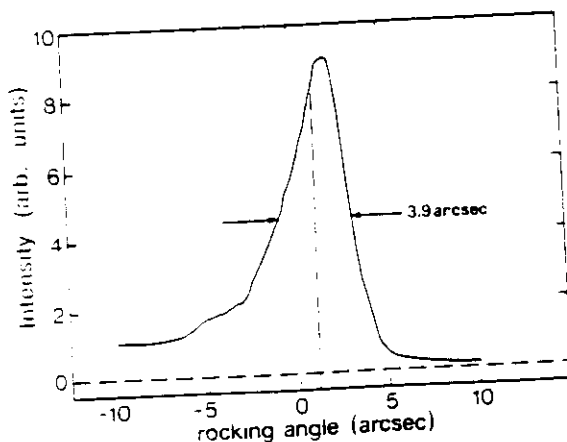
Schematic drawing of the cooled thin silicon crystal assembly. For the sake of clarity, the spacing between the Si foil and Be support was exaggerated, but in reality, both touch each other. When the ring stretches the foil it bends downward at its periphery and a gap is formed between the Si foil and the Be substrate (dotted line).



The Si(333) rocking curve obtained with 3 psi pressure and a small stretching force.

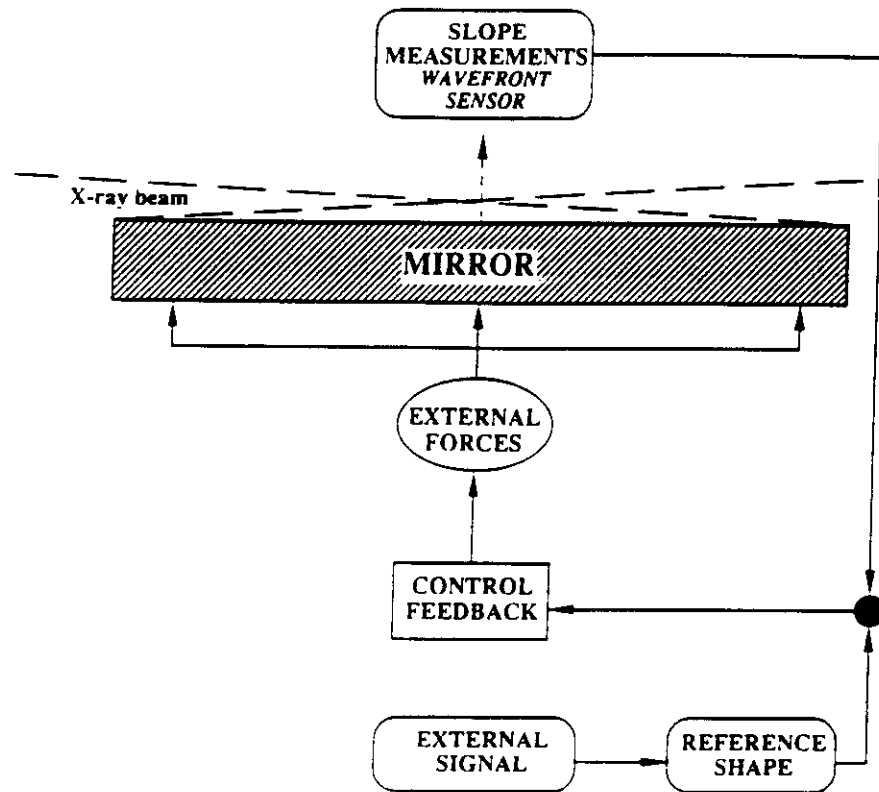


The Si(333) rocking curve obtained without pressure and with 31.4° water temperature. Cold beam.

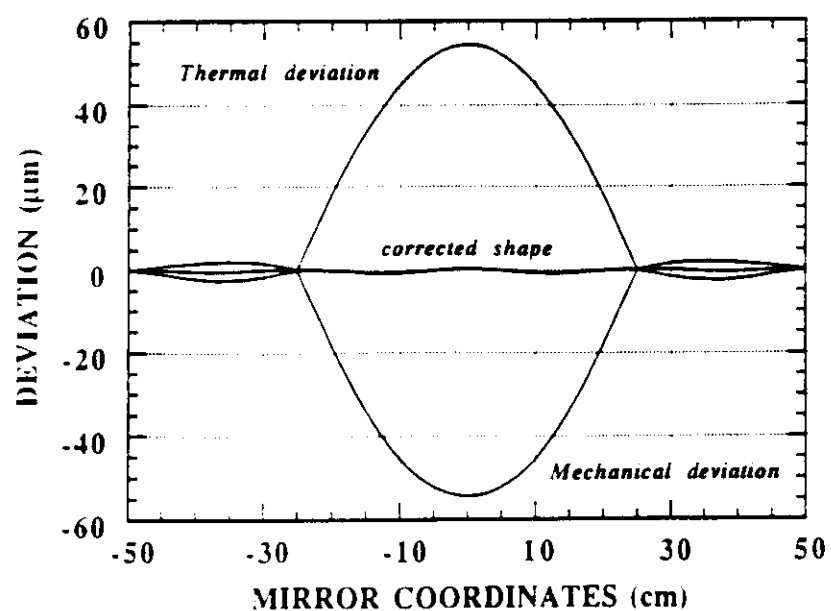


The Si(333) rocking curve obtained with a "warm" beam at 142 mA ring current.

# Adaptive optics

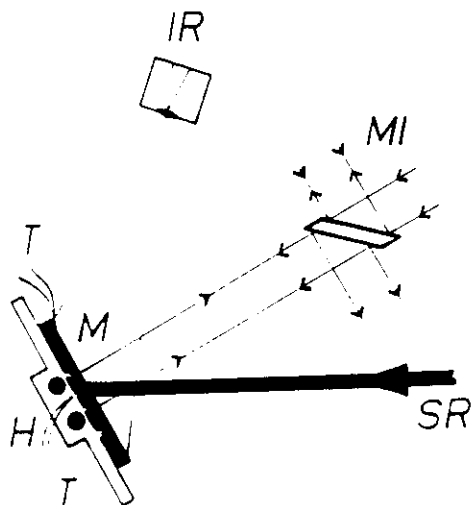


General principle of an adaptive mirror.

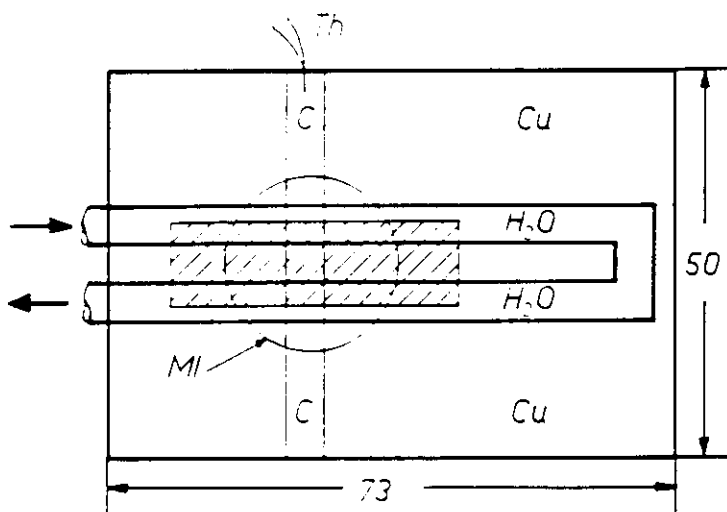


Minimization of the thermal deformation by a mechanical correction by using a set of 11 actuators.

# Experimental configuration for measuring surface thermal distribution and surface slope errors



Side view of the configuration used for this investigation (angle of incidence for the synchrotron radiation:  $28^\circ$ ): M = test mirror, MI = Michelson interferometer, IR = Infrared camera, H = cooled mirror holder (solid circles represent the water channels), SR = incident synchrotron radiation, T = thermocouples.



Top view of the experimental arrangement at the sample holder of dimensions 73 mm  $\times$  50 mm: H<sub>2</sub>O = water channels, C = carbon strip position at sample, Cu = Cu plate, MI = field of view (diameter 22 mm) of the Michelson interferometer, Th = thermocouple touching the side of the test mirror. The shaded rectangle defines the illuminated area.

# REFERENCES

- [1] Nucl. Instr. Meth., Vol. A246 (1986).
- [2] Rev. Sc. Instr., Vol. 60 (1989).
- [3] Nucl. Instr. Meth., Vol. A291 (1990).
- [4] ANL/APS/TM-6 (1990) (Argonne National Lab.)
- [5] Rev. Sc. Instr., Vol. 63 (1992).
- [6] SPIE, Vol. 1739.

